nature neuroscience

ARTICLES

https://doi.org/10.1038/s41593-019-0512-2

Prenatal THC exposure produces a hyperdopaminergic phenotype rescued by pregnenolone

Roberto Frau[1,6], Vivien Miczán[2,3,6], Francesco Traccis[1], Sonia Aroni[1,4], Csaba I. Pongor[5], Pierluigi Saba[1], Valeria Serra[1], Claudia Sagheddu[1], Silvia Fanni[1], Mauro Congiu[1], Paola Devoto[1], Joseph F. Cheer[4], István Katona[3,6] and Miriam Melis[1]*

The increased legal availability of cannabis has led to a common misconception that it is a safe natural remedy for, among others, pregnancy-related ailments such as morning sickness. Emerging clinical evidence, however, indicates that prenatal cannabis exposure (PCE) predisposes offspring to various neuropsychiatric disorders linked to aberrant dopaminergic function. Yet, our knowledge of how cannabis exposure affects the maturation of this neuromodulatory system remains limited. Here, we show that male, but not female, offspring of Δ⁹-tetrahydrocannabinol (THC)-exposed dams, a rat PCE model, exhibit extensive molecular and synaptic changes in dopaminergic neurons of the ventral tegmental area, including altered excitatory-to-inhibitory balance and switched polarity of long-term synaptic plasticity. The resulting hyperdopaminergic state leads to increased behavioral sensitivity to acute THC exposure during pre-adolescence. The neurosteroid pregnenolone, a US Food and Drug Administration (FDA) approved drug, rescues synaptic defects and normalizes dopaminergic activity and behavior in PCE offspring, thus suggesting a therapeutic approach for offspring exposed to cannabis during pregnancy.

The use of cannabis among pregnant women is increasing, with a prevalence rate of 3–16% in Western societies[1–4]. Together with the boom in cannabis marketing and the increased perception of its safety, cross-sectional analyses indicate that cannabis is often recommended to pregnant women as a treatment for morning sickness[5]. Although the use of medical cannabis for nausea and vomiting is approved in several states and countries, no legal distinction or warning for its use during pregnancy is mentioned[6]. Additionally, doctors or other health-care practitioners seldom advise pregnant women about the risks of taking cannabis during pregnancy[6,7].

The main psychoactive ingredient of cannabis, THC, interferes with the endocannabinoid system, which tightly controls progenitor cell proliferation and neuronal differentiation, axon growth and pathfinding, synapse formation and pruning in the developing brain[3,8–10]. Accordingly, four independent longitudinal clinical studies demonstrated that PCE predisposes individuals to a wide array of behavioral and cognitive deficits, including hyperactivity, enhanced impulsivity, loss of sustained attention, increased sensitivity to drugs of abuse[11–13] and susceptibility to psychosis[14]. Notably, all these neuropsychiatric impairments are tied to a dysfunction of dopaminergic signaling[15,16]. While the effects of acute and chronic cannabis use during adolescence and adulthood have been investigated[17–19], the impact of PCE on dopamine neurons within the ventral tegmental area (VTA), key players in motivation, reward and cognition[20], remains to be elucidated.

The 'two-hit' model of psychiatric disorders posits that genetic background and/or environmental insults act as a first hit, perturbing brain development in a manner that leads to susceptibility to the onset of psychiatric symptoms following a second hit. First hits can also lead to endophenotypes such as neurobehavioral deficits[21,22], and characterizing these may help to elucidate altered trajectories of circuit development that increase susceptibility to subsequent challenges[22,23], which may in turn enable prevention of disease emergence. Notably, PCE was recently suggested to act as a first hit by interfering with the known complex developmental functions of endocannabinoid signaling[3,9,23].

Longitudinal studies evaluating the behavioral effects of PCE on offspring have consistently shown that the offspring exhibit increased impulsivity, increased incidence of risk-taking behaviors and vulnerability to psychosis and enhanced sensitivity to drugs of abuse later in life, which can be detected as early as early infancy and throughout child development[11,12,14]. Furthermore, it is predicted that the ratio of affected children developing prenatal THC-induced endophenotypes is likely to be substantially higher[24,25], but the complexity of uncontrollable genetic, environmental and socioeconomic factors in humans makes the determination of causality very difficult. This highlights the advantage of animal models that mimic specific genetic and environmental factors. Here, we tested the hypothesis that PCE triggers molecular and synaptic changes in the VTA, which lead to aberrant dopaminergic activity and behavioral susceptibility to subsequent challenges. In agreement with evidence that the first clinical neuropsychiatric symptoms manifest as early as infancy in PCE offspring[11,14,24], we find that prenatal THC exposure (a model of PCE, hereafter referred to as PCE) engenders 'silent' functional abnormalities, such as impaired sensorimotor gating,

[1]Department of Biomedical Sciences, University of Cagliari, Cittadella Universitaria, Monserrato, Italy. [2]Momentum Laboratory of Molecular Neurobiology, Institute of Experimental Medicine, Hungarian Academy of Sciences, Budapest, Hungary. [3]Faculty of Information Technology and Bionics, Pázmány Péter Catholic University, Budapest, Hungary. [4]Department of Anatomy and Neurobiology, University of Maryland School of Medicine, Baltimore, MD, USA. [5]Nikon Center of Excellence for Neuronal Imaging, Institute of Experimental Medicine, Hungarian Academy of Sciences, Budapest, Hungary. [6]These authors contributed equally: Roberto Frau, Vivien Miczán, István Katona. *e-mail: myriam@unica.it

increased risk-taking and abnormal locomotor responses to THC in juvenile male offspring, that become overt when acutely challenged with THC. Enhanced excitability of VTA dopamine neurons and larger THC-induced dopamine release accompany the PCE-induced endophenotype. Furthermore, we observe altered excitatory–inhibitory balance of VTA dopamine cells along with switched polarity from long-term depression (LTD) to long-term potentiation (LTP) at afferent excitatory synapses. Postnatal administration of pregnenolone, a federal-drug-agency (FDA)-approved drug, which is currently under investigation in clinical trials for cannabis use disorder (ClinicalTrials.gov identifier: NCT02811939), schizophrenia (NCT00728728 and NCT00615511), autism (NCT01881737 and NCT02627508), and bipolar disorder (NCT00223197 and NCT01409096), normalized dopamine neuron excitability, restored synaptic properties and abnormal polarity of synaptic plasticity, as well as THC-induced dopamine release and deficits of sensorimotor gating functions.

Results

PCE induces a distinct behavioral endophenotype. To test the hypothesis that PCE triggers behavioral dysfunctions by altering midbrain dopaminergic activity, we modeled PCE by administering THC (2 mg per kg, subcutaneously (s.c.) once daily) to rat dams during pregnancy (from gestational day (GD) 5 until GD20). This low THC dose does not recapitulate behavioral responses in the cannabinoid tetrad assay or elicits cannabinoid tolerance after repeated administration[26], hence it represents a mild insult without any substantial direct impact on maternal behavior. We did not detect changes in litter size, in maternal and non-maternal behavior, or in changes in offspring body weight at this dose (Supplementary Fig. 1), which indicates that malnutrition and maternal care did not account for any of the observed behavioral effects in the offspring. In terms of human consumption, this dose is equivalent to THC content in mild cannabis cigarettes (joints) (5%)[27], since the average THC content in illicit cannabis preparations has significantly increased in the last two decades (from ~4% to ~12%)[28].

To assess early signs of altered neurodevelopmental trajectories related to PCE endophenotypes, we tested offspring in a series of behavioral tasks under basal conditions and then following an acute THC (2.5 mg per kg, s.c.) or vehicle challenge during the third and fourth postnatal week (postnatal day (PND) 15–28), corresponding to human pre-adolescence. This is because in the clinical staging model, subclinical symptoms are shown before adolescence and early adulthood[29], and a prominent research goal is the identification of such endophenotypes[22]. Moreover, in healthy human subjects, cannabis induces a wide range of deficits that resemble the phenomenology of schizophrenia spectrum disorders[19,30]. Thus, we first investigated whether PCE alters sensorimotor gating functions by using pre-pulse inhibition (PPI) of the acoustic startle reflex. Measures of sensorimotor gating are among the most widely studied physiological markers used in animal models of schizophrenia, and PPI deficits are present in patients with psychotic disorders[31]. Notably, we found that PCE did not affect PPI per se. However, an acute THC challenge disrupted PPI parameters in the PCE group, but remained ineffective in control offspring (Fig. 1a). Because this effect was sex-dependent and specific for this developmental milestone (Fig. 1b; Supplementary Fig. 2a), all experiments hereafter were carried out in male pre-adolescent rats. To test whether PCE induces an endophenotype associated with altered mesolimbic dopamine transmission, we next performed in vivo cerebral microdialysis experiments in the nucleus accumbens shell (NAcS), one of the major target areas of midbrain VTA dopamine neurons (Supplementary Fig. 2b–d). In accordance with our behavioral observations, we did not detect alterations in basal extracellular dopamine levels, but the response to acute THC administration was significantly larger in the PCE offspring group (Fig. 1c), thus indicating that the mesolimbic dopamine system becomes sensitized following maternal THC use. Moreover, we found that THC-induced disruption of PPI significantly and positively correlated with the levels of dopamine in the NAcS (Fig. 1d) and required enhanced mesolimbic dopamine signaling, because an inhibitor of tyrosine hydroxylase (TH) prevented the PPI deficits (Fig. 1e).

We next used open-field tests to examine the effects of PCE on spontaneous locomotor responses to acute THC exposure. No differences were observed between progenies, unless they were acutely treated with THC, as revealed by increased locomotor parameters (Fig. 1f; Supplementary Fig. 3a,b). These effects on spontaneous locomotion were causally dependent on VTA dopamine neuron function, because chemogenetic silencing of dopaminergic neurons via Gi-coupled DREADD (designer receptors exclusively activated by designer drugs; hM4Di) stimulation counteracted the paradoxical hyperlocomotion elicited by THC in PCE offspring (Fig. 1g; Supplementary Fig. 3c,d). Next, we assessed whether the hyperlocomotion and reduced thigmotaxis observed in PCE after a single exposure to THC were associated with behavioral disinhibition. We tested the progenies in the dopamine-dependent suspended wire-beam bridge task, which measures the proclivity to engage in impulsive risk-taking behaviors. This task is operationally defined as the latency to access and move across an unstable bridge and to display stretched-attend postures, an ethologically relevant rodent behavior that occurs during risk assessment. PCE offspring were more prone to cross the bridge (Fig. 1h) and displayed a markedly impaired evaluation of risk assessment (Fig. 1i). Importantly, the propensity of PCE animals to take risks was not associated with alterations in emotional components, because progenies did not differ in the amount of defensive responses to sudden acoustic stimuli measured by startle amplitudes (Supplementary Fig. 3e). Furthermore, they did not display differences in anxiety-related behavior, as assessed by the number of entries and time spent in open or closed arms, or in the number of transitions in the center on the elevated plus maze (Supplementary Fig. 3f,g).

PCE increases dopamine neuron excitability. We next determined the neurobiological mechanisms underlying the heightened dopamine release associated with the behavioral susceptibility observed in PCE offspring. Because type-1 and type-2 cannabinoid (CB_1 and CB_2, respectively) receptors, molecular targets of THC, regulate progenitor cell proliferation in the developing brain[8], we first investigated via confocal microscopy whether PCE alters the number of TH-positive cells or the intensity of TH-immunostaining in the VTA. Neither TH-positive dopamine neuron density (Supplementary Fig. 4a–e) nor TH levels measured in individual cells (Supplementary Fig. 4f) were different. We next probed the function of dopamine neurons by using whole-cell patch-clamp recordings to assess whether PCE-induced changes in physiological properties of dopaminergic neurons promote enhanced release. We performed current-clamp recordings in the lateral portion of the VTA, where cell bodies of the majority of dopamine neurons projecting to the NAcS reside[32], and we verified the TH-immunopositivity of the recorded neurons by post hoc confocal microscopy. Dopamine neurons obtained from PCE offspring showed a different electrophysiological profile: they spontaneously fired at a higher frequency and displayed depolarized resting membrane potentials (Fig. 2a–c). Moreover, PCE dopamine neurons exhibited an overall increased excitability and high maximum spiking frequencies in response to somatically injected currents (Fig. 2d). We also observed a reduced latency to action potential onset, which is the time needed for the first spike appearance in response to the smallest current injection (Fig. 2e). Moreover, a larger proportion of dopamine neurons fired action potentials (16 out of 20, 80%) compared with control offspring (5 out of 21 cells, ~23%; Fig. 2e) and showed enhanced spike fidelity (Supplementary Fig. 5a–d). This is consistent with a decreased spike

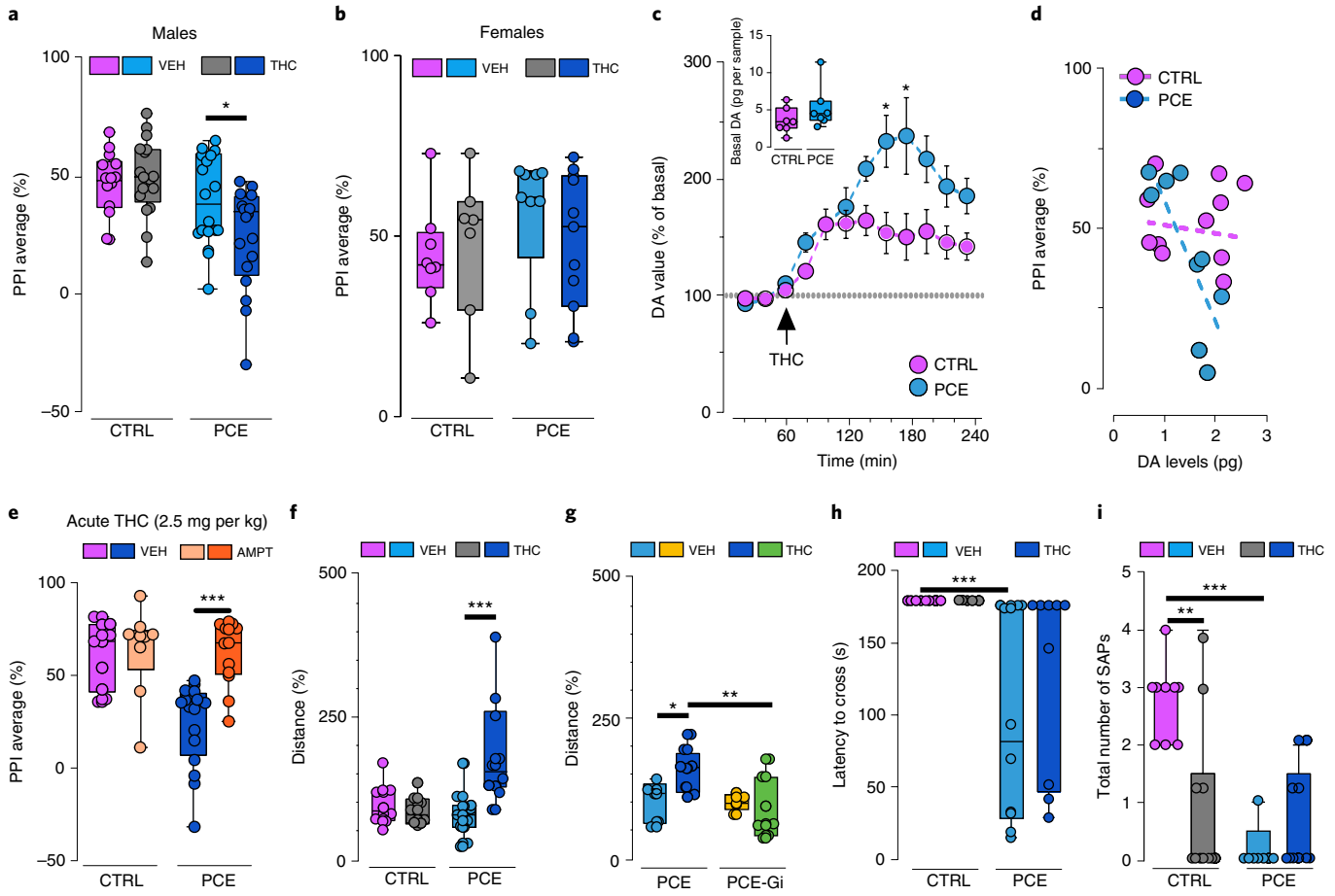

Fig. 1 | PCE elicits behavioral susceptibility to THC in male rat offspring. a,**b**, THC (2.5 mg per kg, s.c.) induces sensorimotor-gating deficits in male (**a**), but not female (**b**), progenies as measured using the PPI index (males, PCE-vehicle (VEH) versus PCE-THC: $^{*}P = 0.037$; control (CTRL)-VEH: $n = 14$; PCE-VEH, PCE-THC: $n = 18$; CTRL-THC: $n = 17$; females: $P = 0.44$ between groups; CTRL-VEH: $n = 8$; PCE-VEH: $n = 9$; CTRL-THC: $n = 7$; PCE-THC: $n = 11$). **c**, THC induces larger dopamine (DA) increase in the NAcS of PCE animals ($^{*}P < 0.05$ between groups; Sidak's test). Data represent the mean ± s.e.m. Inset indicates DA basal values ($P = 0.205$; two-tailed unpaired *t*-test; $n = 7$ per group). **d**, Percentage of PPI values inversely correlates with NAc DA levels of THC-treated PCE offspring. Data are fit by linear regression ($r^2 = 0.62$, $P = 0.01$; CTRL: $n = 11$, PCE: $n = 9$). **e**, DA synthesis inhibition by alpha-methyl-para-tyrosine (AMPT, 200 mg per kg, i.p.) prevents THC-induced PPI deficits in PCE progeny ($^{***}P = 0.0008$, PCE-VEH-THC versus PCE-AMPT-THC; CTRL-VEH-THC, PCE-VEH-THC: $n = 10$ per group; CTRL-AMPT-THC: $n = 9$; PCE-AMPT-THC: $n = 13$). **f**, THC induces hyperlocomotion in PCE offspring ($^{***}P = 0.0008$, CTRL-VEH versus CTRL-THC: $n = 8$ per group; PCE-VEH: $n = 11$, PCE-THC: $n = 10$). **g**, Gi activation prevents THC-induced hyperlocomotion in PCE offspring ($^{*}P < 0.05$, PCE-VEH versus PCE-THC; $^{**}P = 0.003$, PCE-THC versus PCE-Gi-THC; PCE-VEH, PCE-Gi-VEH: $n = 5$ rats per group; PCE-THC: $n = 8$; PCE-Gi-THC: $n = 7$). Distance traveled is the percentage of activity compared with the reference group. **h**,**i**, Crossing latency (**h**; $^{***}P = 0.0006$, PCE versus CTRL) and number of stretched-attend postures (SAPs) (**i**; $^{**}P < 0.01$, CTRL-VEH versus CTRL-THC; $^{***}P < 0.001$, CTRL-VEH versus PCE-VEH) are decreased in PCE offspring. THC does not modify the latency to crossing the bridge (**h**; $P = 0.36$, THC versus VEH group), but reduces SAP number (**i**) only in the CTRL group ($P = 0.02$, THC versus VEH; CTRL-VEH: $n = 8$; CTRL-THC, PCE-THC: $n = 8$ per group; PCE-VEH: $n = 10$). Unless otherwise indicated, graphs depict box-and-whisker plots (including minima, maxima and median values, and lower and upper quartiles) with single values. Data were analyzed using two-way ANOVA followed by Tukey's test.

threshold in response to depolarizing current pulses in neurons from PCE slices (Fig. 2f). In contrast, we did not detect alterations in the after-hyperpolarization period following successive action potentials (Fig. 2g,h), in the membrane capacitance or in inter-spike intervals (Supplementary Fig. 5e,f). Finally, PCE also modified dopamine cell responses to acute THC challenge by increasing spontaneous and evoked activity and enhancing spike fidelity in a dose-dependent and CB_1-receptor-dependent manner (Supplementary Fig. 6). Collectively, these results suggest that PCE biases the dopamine system by changing the intrinsic properties of dopamine neurons and endowing them with a hyper-excitable phenotype, an underlying clinical feature of diverse psychiatric disorders[16,20].

PCE shifts excitatory and inhibitory synaptic weights to dopamine neurons. To further address how PCE affects VTA dopamine neurons, we examined their synaptic properties. First, we observed a robust increase in the excitation-to-inhibition ratio of dopamine neurons from PCE slices (Fig. 3a). To elucidate the underlying mechanisms of this phenomenon, we calculated AMPA/$GABA_A$ and NMDA/$GABA_A$ ratios (Supplementary Fig. 7a–c) and produced input–output curves from the responses measured at different stimulus intensities. A substantial decrease in synaptic inhibition of VTA dopamine cells obtained from PCE rats was revealed (Fig. 3b; Supplementary Fig. 7a–c). To assess whether this change arises from presynaptic mechanisms, we first computed the 1/coefficient of variation^2 ($1/CV^2$) value, which is an independent measure of changes in presynaptic function[33]. We found that PCE markedly decreased the $1/CV^2$ of inhibitory postsynaptic currents (IPSCs) at lower stimulus intensities, which indicated that there was reduced release probability at inhibitory synapses

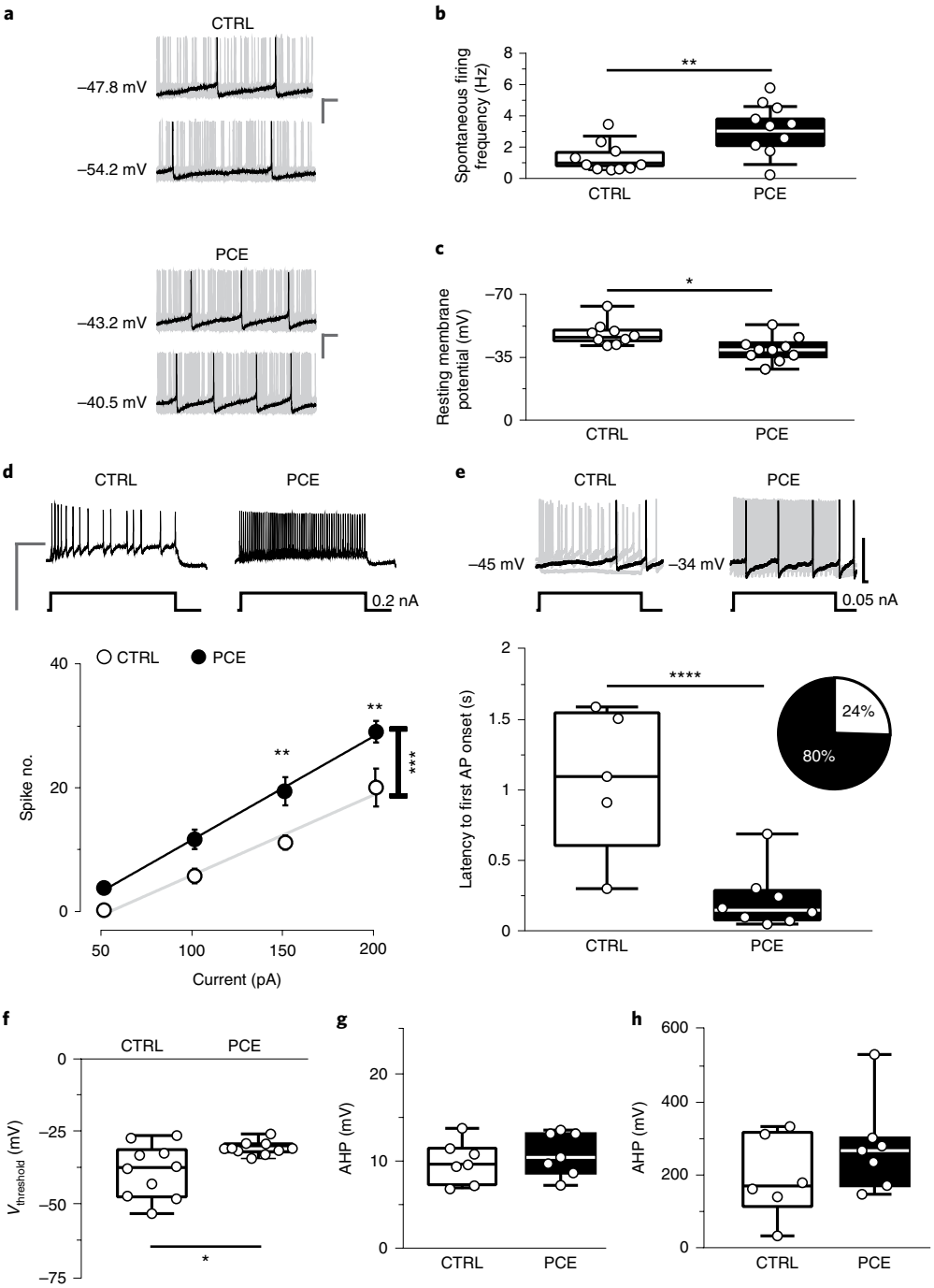

Fig. 2 | PCE enhances pacemaker and evoked activity of VTA dopamine neurons in male rat offspring. a, Representative traces of spontaneous activity of DA neurons in acute slices from CTRL and PCE offspring ($n = 20$ and 21 experiments from PCE and CTRL slices, respectively, were repeated independently with similar results obtained). Calibration bars, 100 ms, 20 mV. **b**,**c**, PCE offspring (n (rat) = 10, n (litter) = 6) show higher spontaneous activity (**b**; $^{**}P = 0.001$ between groups; Welch's correction) and lower resting membrane potentials (**c**; $^{*}P = 0.01$ between groups) compared with CTRL offspring (n (rat) = 10, n (litter) = 6). **d**, PCE DA cells (n (rat) = 10, n (litter) = 6) exhibit increased excitability in response to somatically injected current ($^{***}P = 0.0001$ between groups; two-way repeated-measures ANOVA followed by Bonferroni correction) compared with CTRL cells (n (rat) = 10, n (litter) = 6). Data are represented as average values per animal ± s.e.m. Insets show representative traces of evoked action potentials (APs) in response to maximum current injected. Calibration bar, 400 ms, 100 mV. **e**, Top: representative traces of evoked APs in response to the minimum current injected. Calibration bar, 100 ms, 50 mV. bottom: quantification of the latency of first AP appearance in response to the smallest current injected ($^{***}P < 0.001$ between groups). Inset shows the proportion of cells eliciting APs at 50 pA (CTRL in white, PCE in black). **f**, PCE DA cells exhibit a lower voltage threshold ($^{*}P = 0.015$ between groups). **g**,**h**, PCE does not affect the after-hyperpolarization period (AHP) amplitude (**g**; $P = 0.47$ between groups, not significant (NS)) or AHP duration (**h**; $P = 0.14$ between groups, NS) of DA cells. Unless otherwise indicated, graphs show box-and-whisker plots (including minima, maxima and median values, and lower and upper quartiles) with values averaged per animal and analyzed using two-sided unpaired t-test.

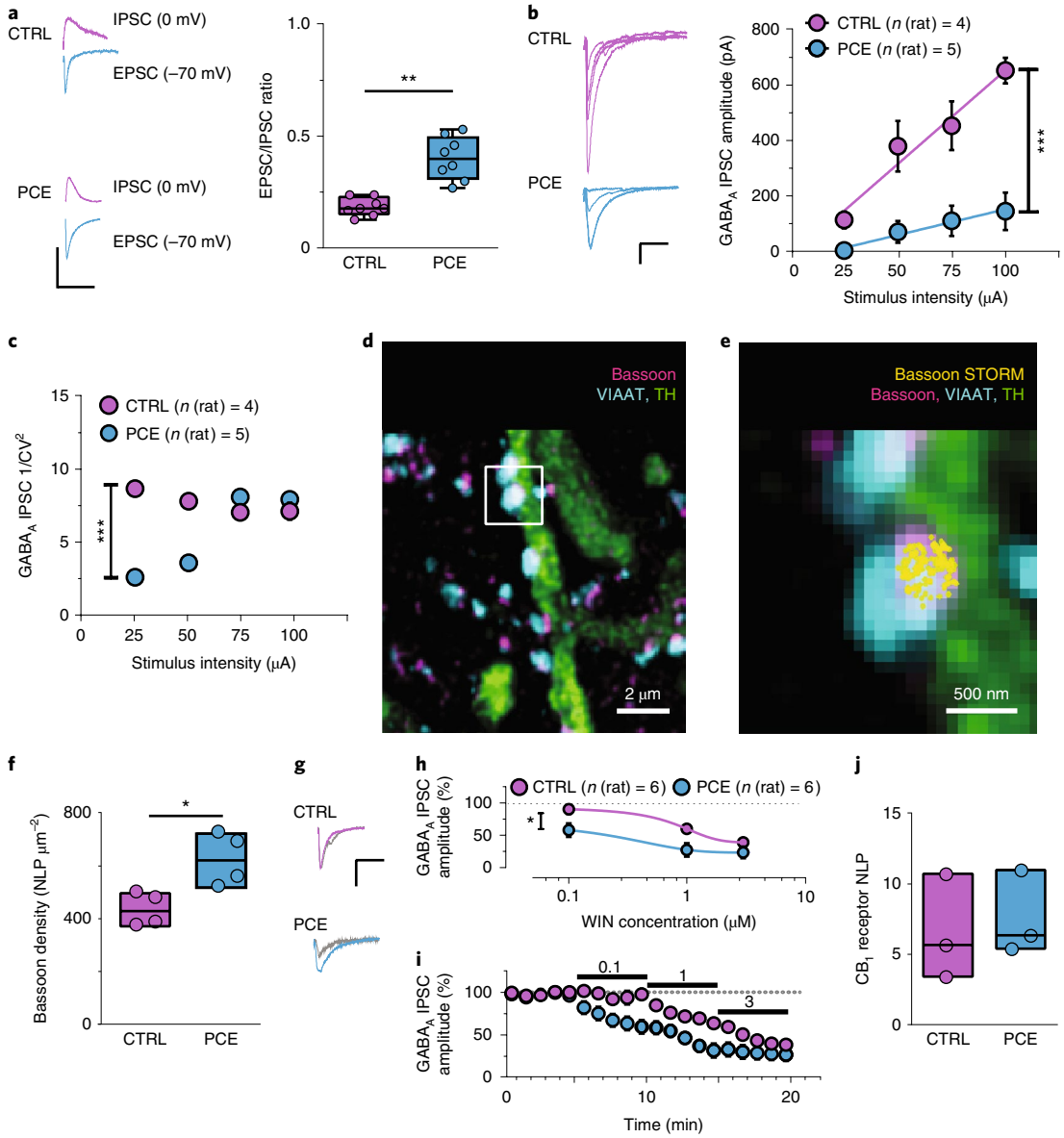

Fig. 3 | PCE reduces synaptic inhibition onto dopamine neurons in male rat offspring. a, Traces (left) and plots (right) of evoked EPSCs and IPSCs recorded from the same DA cells (**$P = 0.002$ between groups; two-sided unpaired *t*-test; *n* (litter) = 5 per group). *n* = 10 experiments from PCE and CTRL slices were repeated independently, with similar results obtained. **b**, Input–output relationships (***$P = 0.0004$ between groups) in CTRL and PCE DA cells. *n* = 5 and 8 experiments from CTRL and PCE slices, respectively, were repeated independently, with similar results obtained. Data represent the mean ± s.e.m. Left panel shows IPSC traces. Calibration bar, 5 ms, 100 pA. **c**, PCE effects on the 1/CV^2 values (***$P = 0.0002$ between groups) from **b**. **d**, Confocal image of VIAAT-containing terminals on a TH$^+$ process. **e**, Enlarged image of an axon terminal (the boxed area in **d)** decorated with bassoon-STORM number of localization points (NLPs) marking the bouton active zone. *n* = 20 images per animal were acquired independently, with similar results obtained. **f**, Bassoon density in VIAAT$^+$ active zones (*$P = 0.030$ between groups; two-sided Mann–Whitney *U*-test; *n* (litter) = 4 per group). **g**, IPSC traces recorded before and after (gray) WIN (0.1 μM) application. Calibration bar, 5 ms, 100 pA. **h**,**i**, Dose–response curves for WIN displaying a larger (**h**; *$P = 0.01$ between groups) and faster effect (**i**; $P = 0.02$ between groups) in PCE versus CTRL groups (*n* (litter) = 4 per group). Numbers on the chart in **i** indicate concentrations of WIN. *n* = 8 and 6 experiments in PCE and CTRL, respectively, were repeated independently, with similar results obtained. Average data per animal ± s.e.m. **j**, CB$_1$ receptor NLPs in VIAAT$^+$ terminals ($P = 0.662$ between groups; two-sided Mann–Whitney *U*-test; *n* (litter) = 3 per group). *n* = 20 images per animal were acquired independently, with similar results obtained. Unless otherwise indicated, graphs show box-and-whisker plots (including minima, maxima and median values, and lower and upper quartiles) with values representing the mean of averaged experiments per animal analyzed with two-way repeated-measures ANOVA followed by Bonferroni's test.

(Fig. 3c). Additionally, PCE increased the paired-pulse ratio (PPR) of GABA$_A$ IPSCs (Supplementary Fig. 7d,e), and decreased the frequency, but not the amplitude, of miniature IPSCs (mIPSCs) (Supplementary Fig. 7f–h).

Recent correlated electrophysiological and super-resolution imaging measurements have uncovered that the clustering of the cytomatrix protein bassoon in the presynaptic active zone is a reliable predictor of presynaptic release probability[34]. This is because an augmented bassoon density inhibits the recruitment of voltage-gated calcium channels required for action-potential-dependent vesicle release[34]. To identify the molecular substrates contributing to the reduced synaptic inhibition of VTA dopamine cells from PCE animals, we combined confocal and stochastic optical reconstruction microscopy (STORM) and quantified bassoon density (measured

with nanometer precision) within identified inhibitory axon terminals impinging on the dendrites of dopamine neurons (Fig. 3d). We observed a substantial increase (by 45%) in the nanoscale density of bassoon at GABAergic synapses obtained from the PCE group (Fig. 3e,f; Supplementary Fig. 8c). In contrast, there was no change in the number and size of inhibitory boutons and their active zones or in vesicular GABA transporter levels (Supplementary Fig. 8). Collectively, these data demonstrate that PCE induces a specific change in the presynaptic nanoarchitecture of inhibitory synapses and suggest that increased molecular crowding at vesicle release sites[34] contributes to the reduced synaptic inhibition of dopamine neurons.

CB_1 receptors are among the most abundant metabotropic regulators of neurotransmitter release probability[35]. Compelling anatomical and electrophysiological evidence shows that CB_1 receptor activation decreases GABA release, thereby sculpting the activity of dopamine signaling[36,37]. Therefore, we tested the hypothesis that enhanced cannabinoid receptor control at inhibitory synapses contributes to reduced synaptic inhibition. The mixed CB_1/CB_2 receptor agonist WIN 55,212-2 (WIN) produced a larger and faster effect on evoked IPSC amplitude recorded from VTA dopamine cells in PCE offspring than in controls (Fig. 3g–i). However, STORM imaging showed no difference in CB_1 receptor levels at GABAergic afferents to dopamine neurons (Fig. 3j). Together, these nanoscale super-resolution data indicate that the ratio of the presynaptic regulatory CB_1 receptors and their molecular effectors in the release machinery complex had shifted so that fewer voltage-gated calcium channels were controlled by a similar number of CB_1 receptors on inhibitory axon terminals in the PCE group compared with the control group. This implies that a saturating dose of the CB_1 receptor agonist WIN should have the same effects on $GABA_A$ IPSC amplitude, and that WIN effects on IPSCs should be faster, which was indeed the case (Fig. 3i). Altogether, these findings demonstrate that PCE induces a molecular reorganization of the active zone that leads to increased presynaptic cannabinoid control along with markedly reduced GABAergic inhibition.

To gain insights into the consequences of PCE on excitatory synaptic transmission, we first measured input–output curves from responses elicited at different stimulus intensities. We found that a larger stimulus intensity is required to recruit the same magnitude of synaptic excitation, which indicates that PCE induces a reduction in the number and/or strength of excitatory inputs terminating on dopamine neurons (Fig. 4a). Indeed, confocal microscopy analysis uncovered a robust (~50%) reduction in the density of type I vesicular glutamate transporter (VGLUT1)-positive excitatory axon terminals contacting TH-positive dopaminergic neurons in the lateral VTA (Supplementary Fig. 9a–c). Conversely, there were no differences in the $1/CV^2$ values of excitatory postsynaptic potentials (EPSCs) (Fig. 4b), in their PPR (Supplementary Fig. 9d,e) or in the frequency of miniature EPSCs (mEPSCs) (Supplementary Fig. 9f,g). In contrast to the lack of presynaptic physiological changes, we observed an increased amplitude of mEPSCs (Supplementary Fig. 9f,h) and longer decay kinetics of postsynaptic AMPA currents in PCE slices compared with control slices (Fig. 4c), which indicates that PCE affected the postsynaptic responsiveness of afferent excitatory synapses of VTA dopamine neurons. Likewise, PCE elicited a larger AMPA/NMDA ratio, with the frequency distribution curve shifted to the right in dopamine cells of PCE offspring, than controls (Fig. 4d–f). Notably, similar increases in the AMPA/NMDA ratio are observed in VTA dopamine neurons of offspring exposed in utero to cocaine or alcohol[38,39]. Thus, potentiated AMPA/NMDA ratios in the postnatal PCE brain directly reflects prenatal drug exposure. We also computed NMDA EPSC decay time kinetics, measured as weighted tau (τ), and found that they were faster in neurons recorded from the PCE progeny (Fig. 5a,b) and were more sensitive to GluN2A blockade (Fig. 5c), which is indicative of an increased ratio of GluN2A/GluN2B subunits in NMDA receptors[38]. Next, we examined the current–voltage relationship (I–V) of AMPA EPSCs. Compared with control animals, the I–V curves of PCE offspring were nonlinear, exhibited inward rectification (Fig. 5d,e) and the GluA2 blocker NASPM reduced AMPA EPSCs to a larger extent (Fig. 5f), thus indicating that there is insertion of calcium permeable (that is, GluA2-lacking) AMPA receptors[38,39]. Taken together, these microscopy and electrophysiological results suggest that PCE delays the molecular and anatomical maturation of excitatory synaptic inputs on VTA dopaminergic neurons, leading to increased postsynaptic responsiveness, a well-known property of developing brain circuits.

A major consequence of reduced inhibitory control of dopamine neurons together with heightened responsiveness to their excitatory inputs might also be a shift in the threshold for synaptic plasticity induction. Pairing low-frequency presynaptic stimulation (LFS; 1 Hz) with postsynaptic membrane depolarization (−40 mV) resulted in the expected LTD of excitatory synapses[40]. In contrast, we found that the very same stimulus protocol elicited a marked LTP in VTA dopamine neurons from PCE animals (Fig. 5g,h), an effect reminiscent of immature glutamatergic synapses.

We next examined whether the synaptic effects of PCE were cell-type-specific in the lateral VTA circuitry. GABA and dopamine neurons, which make up the vast majority of neurons in the lateral VTA[41] (Supplementary Fig. 10a,b), could be reliably distinguished by their morphological and electrophysiological characteristics and by the absence or presence of TH[42] in post hoc immunofluorescence analysis, respectively (Supplementary Fig. 10c–l). While PCE did not affect the excitatory/inhibitory balance, it decreased the AMPA/NMDA ratio (Supplementary Fig. 11a,b). Notably, NMDA EPSC decay times, I–V curves of AMPA EPSCs, PPRs of both AMPA EPSCs and $GABA_A$ IPSCs in putative GABA cells did not differ between progenies (Supplementary Fig. 11c–f). Thus, PCE does not alter the content of GluA2-containing AMPARs or GluN2A-containing NMDARs at these synapses onto VTA putative GABA neurons, but specifically modifies EPSC generation. Collectively, these findings suggest that PCE predominantly affects the synaptic maturation of dopamine cells within the VTA circuitry.

Pregnenolone rescues dopamine function and behavior after PCE. Since preventive strategies to reduce the burden of PCE in offspring are currently not in place[7], the identification of the PCE endophenotype is instrumental in testing therapeutic interventions during the prodromal phases of late-onset psychiatric disorders. In particular, early interventions are needed before the time point at which PCE offspring are of the age of risk for manifesting a disorder to prevent phenoconversion to late-onset disease[14,29,43].

The FDA-approved neurosteroid pregnenolone reverses behaviors such as psychomotor agitation and deficits in PPI that are observed in individuals with schizophrenia[44]. Notably, it also acts as a negative regulator of CB_1 receptor signaling[45]. Therefore, we predicted that a short postnatal treatment of pregnenolone in PCE offspring would be a good candidate for reversing PCE-induced changes in the properties of VTA dopamine neurons and behavior. To assess this, we administered pregnenolone (6 mg per kg, s.c. once daily for 9 days, from PND15 to PND23) or vehicle to PCE offspring, and acute VTA-containing slices were prepared 1 and 2 days following the last administration (Fig. 6a), when pregnenolone is cleared from the brain. Remarkably, pregnenolone rescued LTD at excitatory synapses on dopamine neurons to control levels (Fig. 6b), without affecting synaptic efficacy in control offspring. Moreover, pregnenolone ameliorated PCE-induced dopamine neuron excitability in PCE slices, as assessed by measuring resting membrane potentials (Fig. 6c), and spontaneous (Fig. 6d–f) and evoked firing activity (Fig. 6g,h). Pregnenolone also fully restored the alterations in synaptic properties imposed by PCE on excitatory and

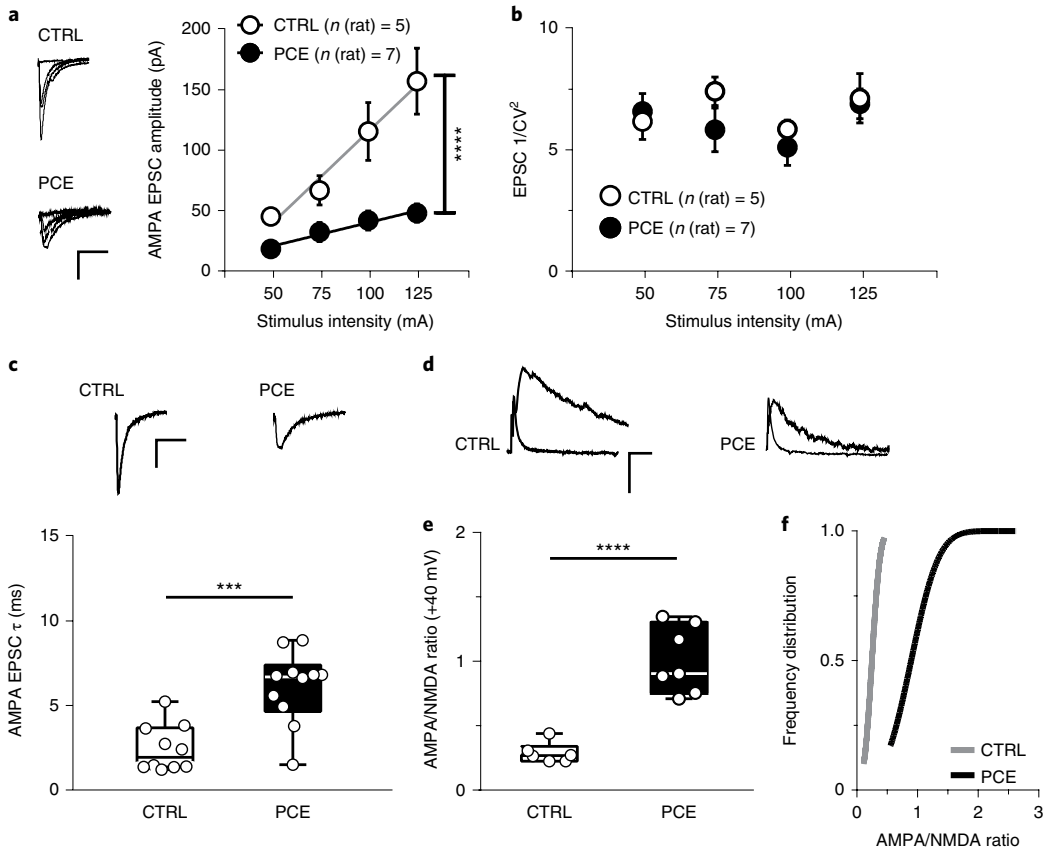

Fig. 4 | Synaptic properties of excitatory inputs onto dopamine neurons are affected by PCE in male rat offspring. a, PCE effects on input–output relationships (****$P < 0.0001$ between groups). $n = 9$ and 7 experiments from PCE and CTRL slices, respectively, were repeated independently with similar results obtained. AMPA EPSC traces are shown on the left. Data represent average values per animal ± s.e.m. **b**, PCE effects on $1/CV^2$ values from **a** ($P = 0.2$ between groups; two-sided Mann Whitney *U*-test). Data represent average values per animal ± s.e.m. **c**, Data from **a** and Fig. 3a (n (litter) = 5 per group) showing that AMPA EPSC decay time kinetic (τ) values differ (***$P = 0.0004$ between groups; two-sided unpaired *t*-test). $n = 15$ and 17 experiments from PCE and CTRL slices, respectively, were repeated independently, with similar results obtained. AMPA EPSC traces (top) were recorded at −70 mV. **d**, AMPA and NMDA EPSC traces recorded from DA neurons held at +40 mV. $n = 9$ and 10 experiments from PCE and CTRL slices, respectively, were repeated independently, with similar results obtained. **e**, PCE effects on the AMPA/NMDA ratio (****$P < 0.0001$ between groups; two-sided unpaired *t*-test). **f**, Cumulative frequency distribution of AMPA/NMDA ratios ($P = 0.0002$ between groups; two-sided Kolmogorov–Smirnov test, $D = 1.0$) recorded from CTRL (n (rat) = 6, n (litter) = 4) and PCE rats (n (rat) = 7, n (litter) = 5). Unless otherwise indicated, graphs show box-and-whisker plots (including minima, maxima and median values, and lower and upper quartiles) with values representing experiments averaged per animal and analyzed with two-way repeated-measures ANOVA. Calibration bars, 10 ms, 50 pA.

inhibitory inputs on dopamine cells (Supplementary Fig. 12). Most importantly, pregnenolone selectively prevented larger acute THC-induced enhancement of dopamine levels in the NAcS (Fig. 6i,j) and THC-induced disruption of somatosensory gating functions in PCE offspring (Fig. 6k). Finally, we found that the mechanism of action of pregnenolone was dissociated from its downstream neurosteroid metabolites (Supplementary Fig. 13). Collectively, these results indicate that pregnenolone prevents PCE-induced hyperdopaminergic states and confers resilience toward heightened acute effects of THC in PCE animals.

Discussion

In the present study, we provide evidence that maternal THC exposure induces multifaceted molecular, cellular and synaptic adaptations that converge into aberrant dopamine function in juvenile male rat offspring. Such persistently enhanced excitability of VTA dopamine neurons is a well-established neurodevelopmental risk factor conferring biased dopamine transmission and vulnerability to discrete psychiatric disorders. This might manifest in aberrant associative learning and abnormal reward processing, and provides an interpretative framework for clinical studies reporting maladaptive behaviors ranging from affective dysregulation to psychosis and addiction vulnerability in the offspring of mothers using cannabis during pregnancy[3,11,14]. It is possible that the decreased expression of dopamine D_2 receptors observed in the amygdala and nucleus accumbens of human PCE offspring[46,47] may be an adaptive response elicited by this hyperdopaminergic state, and may contribute to the vulnerability to psychiatric disorders[15].

We propose that the hyperdopaminergic state and the activity-dependent synapse-specific remodeling identified in the present study are significant neurobiological substrates, which may promote a susceptible endophenotype conferred by maternal cannabis use. This is important because preclinical and clinical studies have also established a prominent and causative role for mesostriatal dopamine dysfunction, in particular elevated dopamine synthesis and release properties, in the pathophysiology of schizophrenia[16]. Notably, positron emission tomography imaging studies have linked a genetic risk for THC-induced psychosis to differential increases of dopamine release by THC[48], a phenomenon exhibiting a high degree of familiarity[49], thus raising the possibility that PCE offspring represent a proportion of cannabis users who are vulnerable to THC-induced psychosis[50]. Hence, PCE might be a risk factor conferring

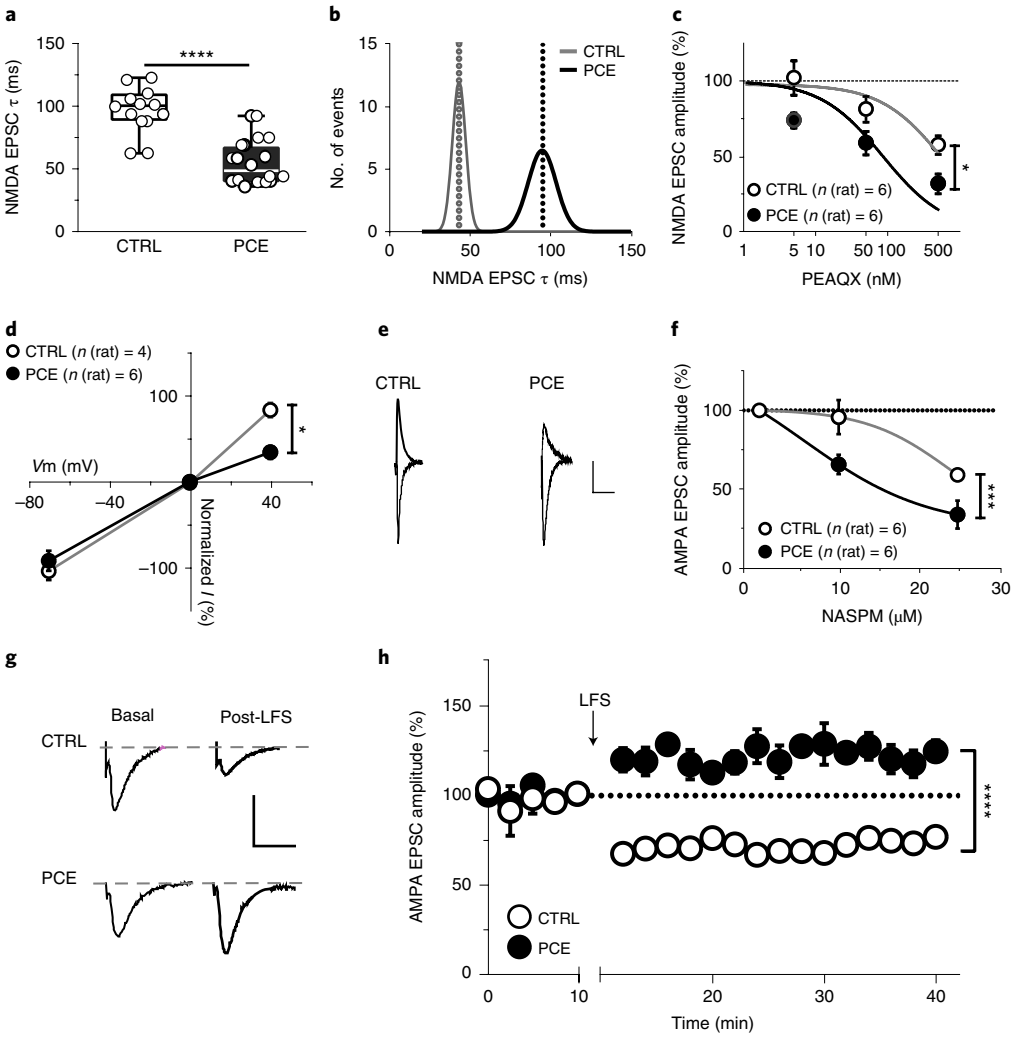

Fig. 5 | PCE enhances postsynaptic responsiveness of dopamine neurons to excitatory stimuli in male rat offspring. a, NMDA receptor EPSC decay time kinetic (weighted tau, τ) values differ (****$P < 0.0001$ between groups; two-sided unpaired *t*-test) between CTRL and PCE slices (*n* (litter) = 6 per group). Box-and-whisker plots (including minima, maxima and median values, and lower and upper quartiles) with circles representing average values per animal. *n* = 18 and 20 experiments from PCE and CTRL slices, respectively, were repeated independently, with similar results obtained. **b**, Bimodal distribution of NMDA receptor EPSC τ values. **c**, Dose–response curves for the GluN2A antagonist PEAQX (*$P = 0.011$ between groups). *n* = 6 experiments per group were repeated independently, with similar results obtained. **d**, Current–voltage relationship (*I*–*V*) plot shows that PCE (*n* (litter) = 4) affects the linearity of *I*–*V* curves (+40 mV; *$P = 0.02$ between groups). **e**, Traces of AMPA EPSCs recorded at −70 and +40 mV from DA neurons in CTRL and PCE offspring. *n* = 11 and 6 experiments from PCE and CTRL slices, respectively, were repeated independently, with similar results obtained. Calibration bar, 10 ms, 50 pA. **f**, Dose–response curves for the GluA2A antagonist NASPM displaying a larger effect (***$P = 0.0002$ between groups) in PCE (*n* (litter) = 2) offspring than in CTRL offspring. *n* = 6 experiments per group were repeated independently, with similar results obtained. **g**, AMPA EPSCs traces recorded at −70 mV before and after pairing low-frequency presynaptic stimulation (LFS; 1 Hz) with postsynaptic membrane depolarization (−40 mV). Calibration bar, 5 ms, 100 pA. **h**, LFS (1 Hz at the arrow) induces LTP (****$P < 0.0001$ between groups) in PCE offspring (*n* (rat) = 5), whereas CTRL DA neurons (*n* (rat) = 4) exhibit LTD. *n* = 7 and 5 experiments from PCE and CTRL slices, respectively, were repeated independently with similar results obtained. Unless otherwise indicated, data are represented as the average of experiments per animal ± s.e.m. analyzed with two-way repeated-measures ANOVA.

increased vulnerability to psychotic experiences as early as childhood[14]. Since PCE-induced dopamine dysregulation may predispose to THC-dependent delusions and hallucinations, PCE may represent a relevant modifiable predictor of transition to a psychotic disorder.

Our findings are consistent with the protective actions of pregnenolone in acute THC intoxication in rodents[45], and in an established mouse model for schizophrenia[44] as a negative regulator of CB_1 receptor signaling. Although pregnenolone metabolites such as progesterone may have direct effects on GABA and NMDA receptors, the observation that inhibition of the converting enzyme 3β-hydroxysteroid dehydrogenase did not modify the protective effects of pregnenolone on PPI disruption induced by acute THC is consistent with the possibility that pregnenolone per se ameliorates PCE-induced physiological and behavioral dysfunctions. Since pregnenolone is a well-tolerated FDA-approved drug, devoid of major side effects[45], our pharmacological treatment has high translational value as a safe and promising therapeutic approach for offspring of mothers who abused marijuana during pregnancy. Our study warrants further investigation into the effects of PCE on other anatomically and functionally heterogeneous dopamine subpopulations with different axonal projections. Indeed, since our recordings were carried out from the lateral portion of the VTA, which largely projects to the lateral NAcS[32], it is likely that these dopamine neurons would mainly project to this region.

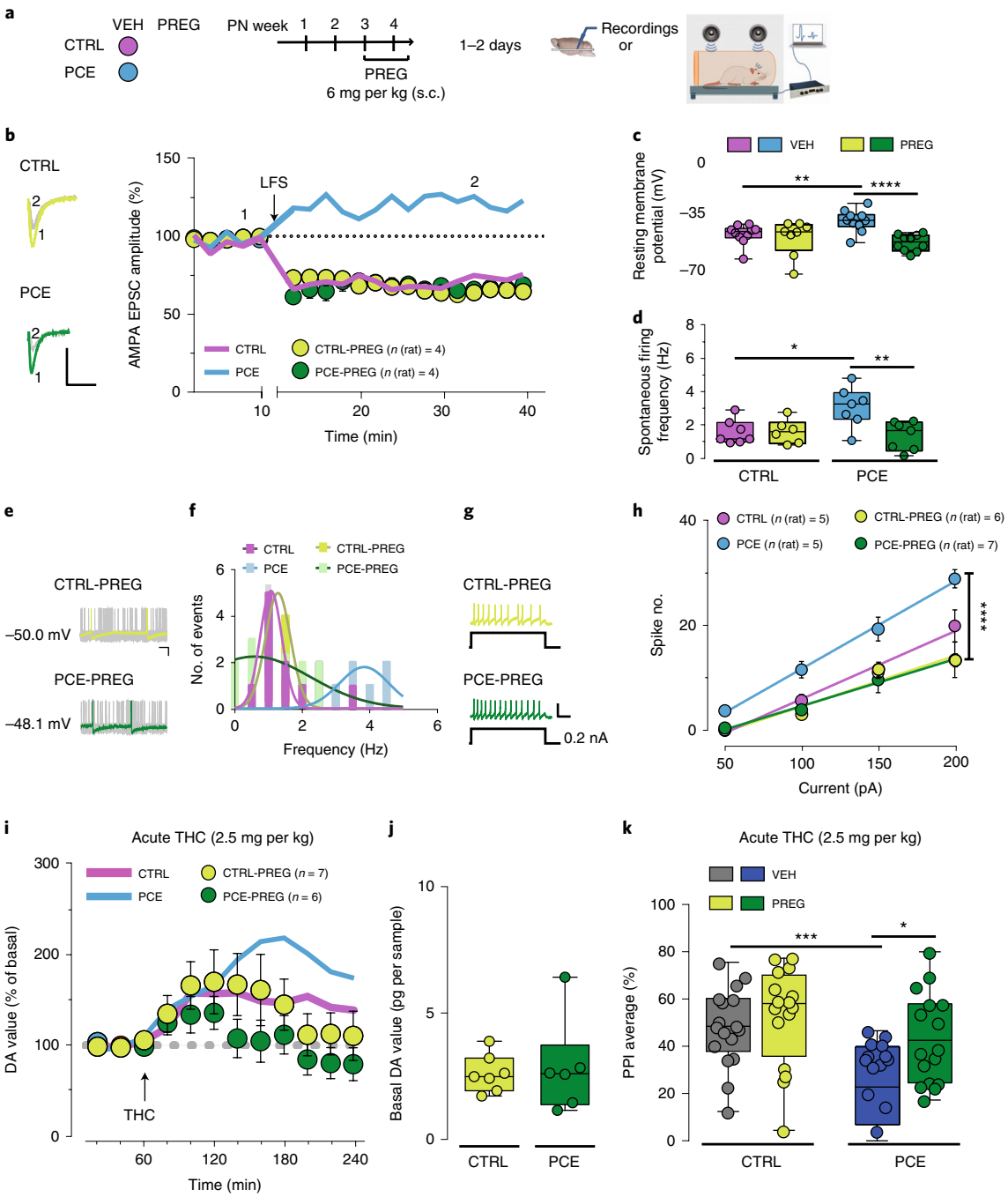

Fig. 6 | Pregnenolone rescues synaptic plasticity, mitigates deficits in dopamine neuron activity and restores behavior in PCE male rat progeny. a, Protocol of pregnenolone (PREG) treatment and analyses. **b**, PREG effects on low-frequency presynaptic stimulation (LFS; 1 Hz at the arrow) ($P = 0.02$, PCE-VEH versus PCE-PREG). Thick lines represent effects from Fig. 5g. Data represent the mean per animal ± s.e.m. Left-hand panel shows traces (−70 mV) from before (1) and after LFS (2). Calibration bar, 5 ms, 100 pA. $n = 6$ experiments per group were repeated independently, with similar results obtained. **c**, Effects of PREG on resting membrane potentials (****$P = 0.0006$, PCE-VEH versus PCE-PREG; **$P < 0.01$, PCE-VEH versus CTRL-VEH; n (litter) = 5 per group). **d**, PREG effects on spontaneous activity (**$P < 0.01$, PCE-VEH versus PCE-PREG; *$P = 0.02$, PCE-VEH versus CTRL-VEH; n (litter) = 5 per group). **e**, Traces from PREG-treated offspring. Calibration bar, 20 ms, 100 pA. $n = 14$ and 12 experiments from PCE and CTRL slices, respectively, were repeated independently, with similar results obtained. **f**, Multimodal distribution of data from **d**. **g**, Traces of evoked firing in PREG-treated offspring. Calibration bar, 400 ms, 100 mV. Numbers of experiments are as in **c**–**h**. **h**, PREG restores evoked firing (****$P < 0.0001$, PCE-VEH versus PCE-PREG; n (litter) = 5 per group). Data represent values averaged per animal ± s.e.m. **i**, PREG attenuates THC effects on NAc DA levels in PCE rats ($P = 0.30$ between groups). Thick lines show data from Fig. 1c. Data represent the mean ± s.e.m. **j**, Basal DA values ($P = 0.768$ between groups; two-sided unpaired t-test). **k**, PREG prevents THC effects on PPI in PCE offspring (*$P = 0.032$, PCE-THC-VEH versus PCE-THC-PREG; ***$P = 0.0004$, CTRL-THC-VEH versus PCE-THC-VEH; Tukey's test; CTRL-THC-VEH: $n = 17$; CTRL-THC-PREG, PCE-THC-VEH, PCE-THC-PREG: $n = 16$; n (litter) = 8 per group). Unless otherwise indicated, box-and-whisker plots (including minima, maxima and median values, and lower and upper quartiles) with circles depicting average data per animal analyzed with two-way repeated-measures ANOVA followed by Sidak's test.

Finally, it is important to emphasize that some of the potentiated state measures of dopamine neurons resemble those described in VTA dopamine neurons of offspring exposed in utero to cocaine or alcohol[38,39]. As physicians caution pregnant women against alcohol and cocaine intake because of their detrimental effects to the fetus, based on our findings, it is our recommendation that they also advise them on the consequences of the use of cannabis during pregnancy. Considering that such preventive strategies do not take place owing to the underestimation of the risks of neurodevelopmental adverse effects associated with maternal cannabis use[6,7], and that cannabis legalization policies move forward worldwide and that conceivably large numbers of children will be prenatally exposed to its ingredients over the next decades, the present findings are critically important for unmasking and highlighting extensive neurobiological maladaptations that increase the vulnerability of at-risk offspring to neuropsychiatric disorders.

Online content

Any methods, additional references, Nature Research reporting summaries, source data, statements of code and data availability and associated accession codes are available at https://doi.org/10.1038/s41593-019-0512-2.

Received: 14 September 2018; Accepted: 11 September 2019;
Published online: 14 October 2019

References

1. *Results from the 2010 National Survey on Drug Use and Health: Summary of National Findings* (Substance Abuse and Mental Health Services Administration, 2011).
2. *Legal Topic Overviews: Possession of Cannabis for Personal Use* (European Monitoring Centre for Drugs and Drug Addiction, 2012).
3. Alpar, A., Di Marzo, V. & Harkany, T. At the tip of an iceberg: prenatal marijuana and its possible relation to neuropsychiatric outcome in the offspring. *Biol. Psychiatry* **79**, e33–e45 (2016).
4. Brown, Q. L. et al. Trends in marijuana use among pregnant and nonpregnant reproductive-aged women, 2002–2014. *JAMA* **317**, 207–209 (2017).
5. Dickson, B. et al. Recommendations from cannabis dispensaries about first-trimester cannabis use. *Obstet. Gynecol.* **131**, 1031–1038 (2018).
6. Volkow, N. D., Compton, W. M. & Wargo, E. M. The risks of marijuana use during Pregnancy. *JAMA* **317**, 129–130 (2017).
7. Jansson, L. M., Jordan, C. J. & Velez, M. L. Perinatal marijuana use and the developing child. *JAMA* **320**, 545–546 (2018).
8. Galve-Roperh, I. et al. Cannabinoid receptor signaling in progenitor/stem cell proliferation and differentiation. *Prog. Lipid Res.* **52**, 633–650 (2013).
9. Maccarrone, M., Guzman, M., Mackie, K., Doherty, P. & Harkany, T. Programming of neural cells by (endo)cannabinoids: from physiological rules to emerging therapies. *Nat. Rev. Neurosci.* **15**, 786–801 (2014).
10. Wu, C. S., Jew, C. P. & Lu, H. C. Lasting impacts of prenatal cannabis exposure and the role of endogenous cannabinoids in the developing brain. *Future Neurol.* **6**, 459–480 (2011).
11. Morris, C. V., DiNieri, J. A., Szutorisz, H. & Hurd, Y. L. Molecular mechanisms of maternal cannabis and cigarette use on human neurodevelopment. *Eur. J. Neurosci.* **34**, 1574–1583 (2011).
12. Huizink, A. C. Prenatal cannabis exposure and infant outcomes: overview of studies. *Prog. Neuropsychopharmacol. Biol. Psychiatry* **52**, 45–52 (2014).
13. De Genna, N. M., Richardson, G. A., Goldschmidt, L., Day, N. L. & Cornelius, M. D. Prenatal exposures to tobacco and cannabis: associations with adult electronic cigarette use. *Drug Alcohol Depend.* **188**, 209–215 (2018).
14. Fine, J. D. et al. Association of prenatal cannabis exposure with psychosis proneness among children in the adolescent brain cognitive development (ABCD) study. *JAMA Psychiatry* **7**, 762–764 (2019).
15. Volkow, N. D., Fowler, J. S., Wang, G. J. & Swanson, J. M. Dopamine in drug abuse and addiction: results from imaging studies and treatment implications. *Mol. Psychiatry* **9**, 557–569 (2004).
16. Grace, A. A. Dysregulation of the dopamine system in the pathophysiology of schizophrenia and depression. *Nat. Rev. Neurosci.* **17**, 524–532 (2016).
17. Bloomfield, M. A., Ashok, A. H., Volkow, N. D. & Howes, O. D. The effects of Δ9-tetrahydrocannabinol on the dopamine system. *Nature* **539**, 369–377 (2016).
18. Bourque, J., Afzali, M. H. & Conrod, P. J. Association of cannabis use with adolescent psychotic symptoms. *JAMA Psychiatry* **75**, 864–866 (2018).
19. Di Forti, M. et al. The contribution of cannabis use to variation in the incidence of psychotic disorder across Europe (EU-GEI): a multicentre case–control study. *Lancet Psychiatry* **6**, 427–436 (2019).
20. Buckholtz, J. W. et al. Mesolimbic dopamine reward system hypersensitivity in individuals with psychopathic traits. *Nat. Neurosci.* **13**, 419–421 (2010).
21. Geschwind, D. H. & Flint, J. Genetics and genomics of psychiatric disease. *Science* **349**, 1489–1494 (2015).
22. Insel, T. R. Rethinking schizophrenia. *Nature* **468**, 187–193 (2010).
23. Heffernan, A. L. & Hare, D. J. Tracing environmental exposure from neurodevelopment to neurodegeneration. *Trends Neurosci.* **41**, 496–501 (2018).
24. Richardson, K. A., Hester, A. K. & McLemore, G. L. Prenatal cannabis exposure—the "first hit" to the endocannabinoid system. *Neurotoxicol. Teratol.* **58**, 5–14 (2016).
25. Young-Wolff, K. C. et al. Trends in self-reported and biochemically tested marijuana use among pregnant females in california from 2009–2016. *JAMA* **318**, 2490–2491 (2017).
26. Wiley, J. L., O'Connell, M. M., Tokarz, M. E. & Wright, M. J. Jr. Pharmacological effects of acute and repeated administration of Δ^9-tetrahydrocannabinol in adolescent and adult rats. *J. Pharm. Exp. Ther.* **320**, 1097–1105 (2007).
27. Mehmedic, Z. et al. Potency trends of Δ9-THC and other cannabinoids in confiscated cannabis preparations from 1993 to 2008. *J. Forensic Sci.* **55**, 1209–1217 (2010).
28. ElSohly, M. A. et al. Changes in cannabis potency over the last 2 decades (1995–2014): analysis of current data in the United States. *Biol. Psychiatry* **79**, 613–619 (2016).
29. McGorry, P. D., Hickie, I. B., Yung, A. R., Pantelis, C. & Jackson, H. J. Clinical staging of psychiatric disorders: a heuristic framework for choosing earlier, safer and more effective interventions. *Aust. NZ J. Psychiatry* **40**, 616–622 (2006).
30. Sherif, M., Radhakrishnan, R., D'Souza, D. C. & Ranganathan, M. Human laboratory studies on cannabinoids and psychosis. *Biol. Psychiatry* **79**, 526–538 (2016).
31. Braff, D. L., Swerdlow, N. R. & Geyer, M. A. Gating and habituation deficits in the schizophrenia disorders. *Clin. Neurosci.* **3**, 131–139 (1995).
32. Lammel, S., Ion, D. I., Roeper, J. & Malenka, R. C. Projection-specific modulation of dopamine neuron synapses by aversive and rewarding stimuli. *Neuron* **70**, 855–862 (2011).
33. Malinow, R. & Tsien, R. W. Presynaptic enhancement shown by whole-cell recordings of long-term potentiation in hippocampal slices. *Nature* **346**, 177–180 (1990).
34. Glebov, O. O. et al. Nanoscale structural plasticity of the active zone matrix modulates presynaptic function. *Cell Rep.* **18**, 2715–2728 (2017).
35. Lovinger, D. M. in *Pharmacology of Neurotransmitter Release* Vol. 184 (eds Südhof, T.C. & Starke, K.) 435–477 (Springer, 2008).
36. Matyas, F. et al. Identification of the sites of 2-arachidonoylglycerol synthesis and action imply retrograde endocannabinoid signaling at both GABAergic and glutamatergic synapses in the ventral tegmental area. *Neuropharmacology* **54**, 95–107 (2008).
37. Melis, M. et al. Enhanced endocannabinoid-mediated modulation of rostromedial tegmental nucleus drive onto dopamine neurons in Sardinian alcohol-preferring rats. *J. Neurosci.* **34**, 12716–12724 (2014).
38. Bellone, C., Mameli, M. & Luscher, C. In utero exposure to cocaine delays postnatal synaptic maturation of glutamatergic transmission in the VTA. *Nat. Neurosci.* **14**, 1439–1446 (2011).
39. Hausknecht, K. et al. Excitatory synaptic function and plasticity is persistently altered in ventral tegmental area dopamine neurons after prenatal ethanol exposure. *Neuropsychopharmacology* **40**, 893–905 (2015).
40. Thomas, M. J., Malenka, R. C. & Bonci, A. Modulation of long-term depression by dopamine in the mesolimbic system. *J. Neurosci.* **20**, 5581–5586 (2000).
41. Yamaguchi, T., Sheen, W. & Morales, M. Glutamatergic neurons are present in the rat ventral tegmental area. *Eur. J. Neurosci.* **25**, 106–118 (2007).
42. Chieng, B., Azriel, Y., Mohammadi, S. & Christie, M. J. Distinct cellular properties of identified dopaminergic and GABAergic neurons in the mouse ventral tegmental area. *J. Physiol.* **589**, 3775–3787 (2011).
43. Marin, O. Developmental timing and critical windows for the treatment of psychiatric disorders. *Nat. Med.* **22**, 1229–1238 (2016).
44. Wong, P., Sze, Y., Chang, C. C., Lee, J. & Zhang, X. Pregnenolone sulfate normalizes schizophrenia-like behaviors in dopamine transporter knockout mice through the AKT/GSK3beta pathway. *Transl Psychiatry* **5**, e528 (2015).
45. Vallee, M. et al. Pregnenolone can protect the brain from cannabis intoxication. *Science* **343**, 94–98 (2014).
46. Wang, X., Dow-Edwards, D., Anderson, V., Minkoff, H. & Hurd, Y. L. In utero marijuana exposure associated with abnormal amygdala dopamine *D2* gene expression in the human fetus. *Biol. Psychiatry* **56**, 909–915 (2004).
47. DiNieri, J. A. et al. Maternal cannabis use alters ventral striatal dopamine D2 gene regulation in the offspring. *Biol. Psychiatry* **70**, 763–769 (2011).
48. Kuepper, R. et al. Delta-9-tetrahydrocannabinol-induced dopamine release as a function of psychosis risk: 18F-fallypride positron emission tomography study. *PLoS One* **8**, e70378 (2013).

49. McGrath, J. et al. Association between cannabis use and psychosis-related outcomes using sibling pair analysis in a cohort of young adults. *Arch. Gen. Psychiatry* **67**, 440–447 (2010).
50. Compton, M. T. et al. Association of pre-onset cannabis, alcohol, and tobacco use with age at onset of prodrome and age at onset of psychosis in first-episode patients. *Am. J. Psychiatry* **166**, 1251–1257 (2009).

Acknowledgements

The authors thank R. Tonini and O. J. Manzoni for discussions and comments on the manuscript, and G. Talani, M. Pignatelli, M. Tuveri, S. Aramo, G. Giua and B. Tuveri for their skillful assistance. The authors are also grateful to L. Barna for his help with STORM microscopy images, and thank Nikon Europe, Nikon Austria and Auro-Science Consulting for kindly providing microscopy support. The present study was supported by the University of Cagliari (RICCAR 2017 and 2018 to M.M.), the Region of Sardinia (RASSR32909 to M.M. and F72F16002850002 to R.F.), the Fondazione Banco di Sardegna (F71I17000200002 to R.F.), the European Molecular Biology Organization (ASTF 371-2016 to C.S.), the Fondazione Zardi Gori (to C.S.), the National Institutes of Health (R01DA022340 to J.F.C., R01NS099457 to I.K. and R01DA044925 to J.F.C., M.M. and I.K.), the Hungarian Academy of Sciences Momentum Program (LP-54/2013 to I.K.), and the National Research, Development and Innovation Office of Hungary (VKSZ-14-1-2015-0155 to I.K.). The project was also funded by the Ministry of National Economy for STORM super-resolution microscopy (VEKOP-2.3.3-15-2016-00013 to I.K.).

Author contributions

R.F. and F.T. designed and performed the behavioral experiments and analyzed the data. S.F. and V.S. carried out behavioral observations. F.T. and V.S. prepared the figures. V.M. and C.I.P. carried out the confocal imaging and STORM experiments, the corresponding data analyses and prepared the figures. P.S. and P.D. carried out the cerebral microdialysis experiments and analyzed the data. M.C. and V.S. designed and performed the maternal observation experiments. C.S., V.S. and S.A. performed the chronic drug administration treatment. S.A. performed the DREADD experiments. J.F.C. designed the DREADD experiments and contributed to manuscript preparation. I.K. designed the confocal and STORM experiments, analyzed and supervised the imaging data and wrote the manuscript. M.M. conceived, designed and supervised the project, performed patch-clamp recordings, analyzed the data, prepared the figures and wrote the manuscript.

Competing interests

The authors declare no competing interests.

Additional information

Supplementary information is available for this paper at https://doi.org/10.1038/s41593-019-0512-2.

Correspondence and requests for materials should be addressed to M.M.

Peer review information *Nature Neuroscience* thanks Camilla Bellone, Paul Kenny, and the other, anonymous, reviewer(s) for their contribution to the peer review of this work.

Methods

Animals. All procedures were performed in accordance with the European legislation EU Directive 2010/63 and the National Institutes of Health Guide for the Care and Use of Laboratory Animals and were approved by the Animal Ethics Committees of the University of Cagliari and by the Italian Ministry of Health (authorization numbers: 659/2015-PR and 725/2019-PR) and by the Institutional Animal Use and Care Committee at the University of Maryland (0617002). We made all efforts to minimize pain and suffering and to reduce the number of animals used. Primiparous female Sprague–Dawley (Envigo) rats (bred with males) were used as mothers and single housed during pregnancy. Long–Evans dams expressing Cre recombinase under the control of the *TH* promoter (*TH*::Cre) were used for the DREADD experiments. THC or vehicle was administered (2 mg per kg, 2 ml per kg, s.c. once per day) from GD5 until GD20. Offspring were weaned at ~PND21 and maintained without any further manipulation in standard conditions of temperature (21 ± 1 °C) and humidity (60%) on a normal 12-h light–dark cycle with access to food and water until the experimental day (PND15–28). We did not use more than two males from each litter for the same experiment to control for litter effects. All the additional male pups in each litter were used for other experiments (that is, cerebral microdialysis, behavioral paradigms, STORM analysis and different electrophysiological protocols) to minimize the total number of animals used for the study.

Surgical procedures. *TH*::Cre-positive offspring were stereotaxically injected under isoflurane (3% induction, 1–2% maintenance) with a Cre-dependent adeno-associated virus expressing an inhibitory DREADD construct (AAV5-DIO-hM4D(Gi)-mCherry (PCE-Gi)) or control virus (AAV5-DIO-mCherry (PCE)) to target dopamine neurons in the VTA at PND7. Viruses were injected at a volume of 0.5 µl per side and a rate of 0.1 µl min^{-1} in the VTA (anterior–posterior: −4.2, medial–lateral: ± 0.6 mm from bregma, and dorsal–ventral: −5.25 mm from the cortical surface) with a Hamilton syringe. Injection needles were left in place for 5 min after the injection to ensure adequate viral delivery.

Behavioral analyses. *Maternal behavior observation.* The behavior of each dam was assessed from PND1 to PND20 by an observer blinded to the experimental groups until the analyses of data. The observation was performed five times per day at 9:00, 11:30, 13:30, 15:00 and 17:00 during the light phase (lights on at 7:00) and consisted of 3 trials of instantaneous observation for a total of 15 observations per day and a total 300 observations per dam. Behavioral parameters such as retrieval, arched-back, blanket and passive nursing, pup licking (regarded as maternal behaviors), self-grooming, eating, drinking, rearing, moving, resting, standing out of the nest (considered as non-maternal behaviors) were scored. Observations strictly followed a previously published detailed analysis protocol[51]. Briefly, the behaviors were recorded using dichotomous scores of 0 and 1, where 0 was assigned when the behavior was not present, and 1 was assigned when it was present. Data were expressed as a percentage of observations of maternal or non-maternal behavior.

Startle reflex and PPI. Startle reflex and PPI were tested as previously described[52]. Briefly, the apparatus (Med Associates) consisted of four standard cages placed in sound-attenuated chambers with fan ventilation. Each cage consisted of a Plexiglas cylinder 5 cm in diameter, mounted on a piezoelectric accelerometric platform connected to an analog–digital converter. Two separate speakers conveyed background noise and acoustic bursts, each one properly placed so as to produce a variation of sound within 1 dB across the startle cage. Both speakers and startle cages were connected to a main personal computer, which detected and analyzed all chamber variables using specific software. Before each testing session, acoustic stimuli and mechanical responses were calibrated via specific devices supplied by Med Associates. The testing session featured a background noise of 70 dB and consisted of an acclimatization period of 5 min, followed by three consecutive sequences of trials (blocks). Unlike the first and the third block, during which rats were presented with only five pulse-alone trials of 115 dB, the second block consisted of a pseudorandom sequence of 50 trials, including 12 pulse-alone trials, 30 trials of pulse preceded by 74, 78 or 86 dB pre-pulses (10 for each level of pre-pulse loudness), and 8 no-stimulus trials, where only the background noise was delivered. Inter-trial intervals were selected randomly between 10 and 15 s. The percentage PPI value was calculated using the following formula: 100 − ((mean startle amplitude for pre-pulse pulse trials/mean startle amplitude for pulse alone trials) × 100). PPI values related to different pre-pulse levels were collapsed, given that no interactions were found between pre-pulse levels throughout the study.

Locomotor activity. Locomotor behaviors of Sprague–Dawley rats and Long–Evans *TH*::Cre rats were tested in two different facilities at the University of Cagliari and at the University of Maryland School of Medicine, respectively. Rats were placed in the center of a novel, square open-field (dimensions of 42-cm long × 42-cm wide × 30-cm high) and their behavior was monitored for 40 min and collected every 10 min. Analysis of locomotor activity of Sprague–Dawley rats and Long–Evans *TH*::Cre rats were performed using an Omnitech Digiscan monitoring system (Omnitech Digiscan cages) and Ethovision (Noldus Instruments), respectively. Behavioral measurements included the assessment of the total distance traveled (in cm), and the periphery and center time, respectively, calculated as the durations of time spent along the perimeter of the walls (a 20-cm-wide external square frame) or in the center of the arena (an internal square measuring 20 × 20 cm). To minimize differences in baseline spontaneous locomotor activity (that is, distance traveled), we normalized the data to their reference group (for example, control-vehicle and PCE-vehicle). For the DREADD experiments, open-field testing was performed 30 min following a systemic administration of clozapine-*N*-oxide (3 mg per kg, 2 ml intraperitoneally (i.p.)) to engage VTA Gi-DREADDs.

Elevated plus maze. The test was performed as previously described[53]. Briefly, we used a black Plexiglas apparatus consisting of two opposing open arms (length of 40 cm, width of 9 cm) and two closed arms (wall height of 15 cm), which extended from a central square platform (9 × 9 cm), positioned 70 cm from the ground. Rats were individually placed on the central platform facing the open arm. Behavior was recorded for 5 min. Measures included the number of entries and duration in the open and closed arms and in the central platform, frequencies of stretch-attend postures and head dips (defined as previously described).

Wire-beam bridge test. Testing was performed using a variant of a previously detailed protocol[54,55], specifically adapted for rats. The apparatus consists of two 156-cm high Plexiglas platforms connected by a horizontal, flexible wire-beam (100-cm long). A 52-cm high Plexiglas wall was placed 3 cm from the edge of one platform to make the starting position uncomfortable and to promote movement. The bridge consisted of 2 parallel beams (0.1-cm thick) perpendicularly connected by 34 equally distanced cross-ties (3-cm long). It was modestly flexible, with a downward deflection of 2 cm per 100-g load at the center point. Rats were individually placed in the start position, and the latency to cross and reach the other platform was recorded. The duration of overall immobility and number of crossings on ties were also monitored.

Cerebral microdialysis. Rats were anesthetized with Equithesin and placed in a Kopf stereotaxic apparatus. In-house constructed vertical microdialysis probes (AN 69-HF membrane, Hospal-Dasco; cut-off 40,000 Dalton, 3-mm dialyzing membrane length) were implanted in the NAcS (from bregma: anterior–posterior: + 1.5; lateral: ± 0.7; ventral: −7.0) according to atlas coordinates[56], which were empirically corrected after a pilot experiment. Rats were given antibiotic therapy (enrofloxacin, Bayer HealthCare) and allowed to recover in their home cages before testing. The day after probe implantation, artificial cerebrospinal fluid solution (ACSF; 147 mM NaCl, 4 mM KCl, 1.5 mM $CaCl_2$, 1 mM $MgCl_2$, pH 6–6.5) was pumped through the dialysis probes at a constant rate of 1.1 µl min^{-1} via a CMA/100 microinjection pump (Carnegie Medicine). Samples were collected every 20 min and immediately analyzed for dopamine content by high-performance liquid chromatography with electrochemical detection, as previously described[57]. When a stable baseline was obtained (three consecutive samples with a variance not exceeding 15%), THC (2.5 mg per kg, 2 ml per kg) was i.p. administered, and sample collection continued for 2 h. On completion of the testing, rats were killed via an Equithesin overdose, the brains were removed and sectioned using a cryostat (Leica CM3050 S) into 40-µm thick coronal slices to verify the anatomical locations of dialysis probes.

Electrophysiological recordings. The preparation of posterior VTA slices was performed as previously described[58]. Briefly, a block of tissue containing the midbrain was obtained from male offspring deeply anesthetized with isoflurane and the tissue sliced in the horizontal plane (300 µm) with a vibratome (Leica) in ice-cold low-Ca^{2+} solution containing the following (in mM): 126 NaCl, 1.6 KCl, 1.2 NaH_2PO_4, 1.2 $MgCl_2$, 0.625 $CaCl_2$, 18 $NaHCO_3$ and 11 glucose. Slices were transferred to a holding chamber with ACSF (37 °C) saturated with 95% O_2 and 5% CO_2 containing the following (in mM): 126 NaCl, 1.6 KCl, 1.2 NaH_2PO_4, 1.2 $MgCl_2$, 2.4 $CaCl_2$, 18 $NaHCO_3$ and 11 glucose. Slices were allowed to recover for at least 1 h before being placed, as hemislices, in the recording chamber and superfused with ACSF (36–37 °C) saturated with 95% O_2 and 5% CO_2. Cells were visualized using an upright microscope with infrared illumination (Axioskop FS 2 plus, Zeiss), and whole-cell patch-clamp recordings were made using an Axopatch 200B amplifier (Molecular Devices). Recordings were carried out in the lateral portion of the posterior VTA (Supplementary Fig. 10a,b). Voltage-clamp recordings of evoked IPSCs and current-clamp recordings were made with electrodes filled with a solution containing the following (in mM): 144 KCl, 10 HEPES buffer, 3.45 BAPTA, 1 $CaCl_2$, 2.5 Mg_2ATP and 0.25 Mg_2GTP, pH 7.2–7.4, 275–285 mOsm. All $GABA_A$ IPSCs were recorded in the presence of 2-amino-5-phosphonopentanoic acid (AP5; 100 µM), 6-cyano-2,3-dihydroxy-7-nitro-quinoxaline (10 µM), strychnine (1 µM) and eticlopride (100 nM) to block NMDA, AMPA, glycine and dopamine-D_2-receptor-mediated synaptic currents, respectively. As previously described[58], this solution had no effect on the holding current of the dopamine cells. Current-clamp experiments were performed in the absence of any pharmacological blocker, that is, in regular ACSF. Experiments were begun only after series resistance had stabilized (typically 10–30 MΩ), which was monitored by a hyperpolarizing step of −4 mV at each sweep every 10 s. Data were excluded when the resistance changed >20%. Voltage-clamp recordings of

evoked EPSCs were made with electrodes filled with a solution containing the following (in mM): 117 caesium methanesulfonic acid, 20 HEPES, 0.4 EGTA, 2.8 NaCl, 5 TEA-Cl, 0.1 mM spermine, 2.5 Mg_2ATP and 0.25 Mg_2GTP, pH 7.2–7.4, 275–285 mOsm. Picrotoxin (100 µM) was added to the ACSF to block $GABA_A$-receptor-mediated IPSCs. In addition, random experiments were performed with an internal solution that contained biocytin (0.2%) to allow for subsequent immunocytochemical detection of TH[37] (Supplementary Fig. 10e–g). Series and input resistance were monitored continuously online with a 5-mV depolarizing step (25 ms). Data were filtered at 2 kHz, digitized at 10 kHz and collected online with acquisition software (pClamp 10.2, Molecular Devices). Dopamine neurons from the lateral portion of the posterior VTA were identified according to previously published criteria[58] as follows: cell morphology and anatomical location (that is, medial to the medial terminal nucleus of the accessory optic tract; Supplementary Fig. 10a,b); slow pacemaker-like firing rate (<5 Hz); long action potential duration (>2 ms; Supplementary Fig. 10d); and the presence of a large hyperpolarization-activated current (I_h > 150 pA)[59], which was assayed immediately after break-in using 13 incremental 10-mV hyperpolarizing steps (250 ms) from a holding potential of −70 mV (Supplementary Fig. 10c). Putative GABA neurons of the lateral posterior VTA were identified by their morphology, the absence of I_h and a short action potential duration (<2 ms) (Supplementary Fig. 10h,i). In addition, random experiments were performed with an internal solution containing biocytin (0.2%) to allow for subsequent immunocytochemical detection of TH[37], since GABA cells are negative for TH (Supplementary Fig. 10j–l).

Spike fidelity was measured as the reliability of eliciting an action potential in response to somatically injected current (50–200 pA); the jitter, which is equal to the standard deviation of the latency to elicit the first action potential, inversely correlates with the spike fidelity, as the smaller the jitter the higher degree of temporal precision exhibited by the cell. A bipolar, stainless steel stimulating electrode (FHC) was placed ~100–200 µm rostral to the recording electrode and was used to stimulate at a frequency of 0.1 Hz. Paired stimuli were given with an interstimulus interval of 50 ms, and the ratio between the second and the first postsynaptic currents (PSC2/PSC1) was calculated and averaged for a 5-min baseline[58]. NMDA EPSCs were evoked while holding cells at +40 mV. The AMPA EPSC was isolated after bath application of the NMDA antagonist D-AP5 (100 µM). The NMDA EPSC was obtained by digital subtraction of the AMPA EPSC from the dual (AMPA + NMDA-mediated) EPSC[60]. The values of the AMPA/NMDA ratio might be underestimated, since the experiments were performed in the presence of spermine in the recording pipette. The spontaneous mEPSCs and mIPSCs were collected in the presence of lidocaine (500 µM) or tetrodotoxin (1 µM) and analyzed (120 sweeps for each condition, 1 s per sweep) using Mini Analysis (Synaptosoft). To accurately determine the miniature PSC amplitude, only events that were >8 pA were accepted for analysis (rise time <1 ms, decay time <3 ms). The choice of this cut-off amplitude for acceptance of miniature PSCs was made to obtain a high signal-to-noise ratio. Then, each event was also visually inspected to prevent noise affecting the analysis. Experiments were performed blinded to the experimental group.

Immunostaining. For a detailed protocol, see a previous study[61]. Rats were transcardially perfused with 4% (m/v) paraformaldehyde (PFA) or immersion-fixed in 4% PFA overnight, and 20, 40 or 50 µm-thick sections of the midbrain were cut using a Leica VT-1000S Vibratome in phosphate buffer (PB). Immunostaining was performed in a free-floating manner. After extensive washing in PB and 0.05 M Tris-buffered saline (TBS, pH 7.4), slices were blocked and permeabilized with 5% (v/v) normal donkey serum (Sigma) and 0.3% (v/v) Triton X-100 (Sigma) in TBS for 45 min, then they were incubated in primary antibodies (see Supplementary Table 1) in TBS while rinsed on an orbital shaker. Sections were then washed in TBS and incubated with the appropriate secondary antibodies (see Supplementary Table 1) supplemented with 4,6-diamidino-2-phenylindole (DAPI; 1:1,000), if needed, then extensively washed in TBS and PB.

For confocal imaging, sections were mounted in VectaShield (Vector Laboratories) or Prolong Diamond Antifade Mounting Medium (Invitrogen). Confocal imaging was performed on the samples, and TH-positive cell density and TH-immunofluorescence intensity were calculated on the images within the region of interest (ROI). VGLUT1 and VIAAT inputs of the filled dopaminergic cells were counted in a ~1-µm neighborhood of the cells, and input density was calculated based on the surface of the processes. Objects with a volume lower than 0.02 μm^3 were considered as noise and excluded from the analysis.

For STORM imaging, sections were post-fixed in 4% PFA for 10 min and washed in PB. Samples were then mounted and dried on acetone-cleaned no. 1.5 borosilicate coverslips.

Correlated confocal and STORM imaging. Samples were covered with freshly prepared STORM imaging medium as previously described[62] and contained 0.1 M mercaptoethylamine, 5% (m/v) glucose, 1 mg ml^{-1} glucose oxidase and catalase (2.5 µl ml^{-1} of aqueous solution from Sigma, approximately 1,500 U ml^{-1} final concentration) in Dulbecco's PBS (Sigma). Coverslips were sealed with nail polish. Imaging started after 10 min and was performed for up to 3 h. Images were acquired using a Nikon Ti-E inverted microscope equipped with a Nikon N-STORM system, CFI Apo TIRF ×100 objective (1.49 numerical aperture), a Nikon C2 confocal scan head and an Andor iXon Ultra 897 EMCCD (with a cylindrical lens for astigmatic 3D-STORM imaging[63]). Nikon NIS-Elements AR software with the N-STORM module was used to control the imaging process. A 300-mW laser (VFL-P-300-647, MPB Communications) fiber-coupled to the laser board of the microscope setup was used for STORM imaging. The field of view was selected using the live EMCCD image with a 488-nm illumination, and VIAAT-positive axon terminals impinging on TH-positive cell bodies and dendrites were selected. A three-channel confocal stack (512 × 512 × 15 pixels, 78 × 78 × 150 nm resolution) was then collected using 488-nm, 561-nm and 647-nm excitations. After brief bleaching, direct STORM imaging was performed with 10,000 cycles of 30 ms of exposure, with continuous low-power activator laser (405 nm) and maximal power reporter laser (647 nm) using a STORM filter cube (Nikon) and the EMCCD camera.

Correlated confocal and STORM image processing. Confocal image stacks were deconvolved with 100 iterations of the classic maximum likelihood estimation algorithm in Huygens software (SVI). STORM image processing was performed using the N-STORM module of the NIS-Elements AR. The peak detection threshold was set to 1,000 gray levels. Correlated confocal and STORM image analysis was performed using the software VividSTORM[61]. The data from the two imaging modalities were manually aligned based on the correlated STORM and confocal channels. One axon terminal was selected per image from the center of the field of view. The borders of the axon terminals and the outline of the active zones (for CB1 STORM and bassoon STORM, respectively) were delineated using the Morphological Active Contour Without Edges (MACWE) algorithm[61] with the appropriate confocal channels. STORM localization points (LPs) belonging to the ROI were stored and counted and were normalized to the overall density of LPs per image. The size of the active zone was determined from the active contour ROIs, and the density of bassoon staining in the active zone was calculated by dividing the bassoon number of LPs and the active zone size. The size of the axon terminals was also determined with the MACWE method using the VIAAT confocal channel, and the sum intensity of the VIAAT confocal staining was calculated in the ROIs to estimate transporter levels. Figures were prepared using Photoshop CS5 (Adobe Systems). All images were modified in the same way for all treatment groups during preparation of the figures to ensure equal comparison.

Statistical analyses. No statistical methods were used to predetermine the number of animals and cells required. Sample sizes were estimated based on previous experience and are similar to those reported in previous publications[37,64,65] and generally employed in the field. The animals were randomly assigned to each group for the prenatal pharmacological treatment or behavioral tests. Statistical analyses were conducted using GraphPad Prism 6. Statistical outliers were identified using Grubb's test ($\alpha = 0.05$) and excluded from analyses. Datasets were tested for normality using the Kolmogorov–Smirnov test, and differences between animals within a treatment group were calculated using the Kruskal–Wallis test to determine the appropriate statistical method. For STORM imaging, the mean values of each animals were used in the statistical analyses, differences between the groups were determined using Mann–Whitney *U*-tests. Data always met the assumptions of the applied statistical probes. Electrophysiological data were analyzed using two-way ANOVA for repeated measures (treatment × time) or one-way ANOVA or Student's *t*-test when appropriate, followed by Sidak's, Dunnett's or Bonferroni's post hoc test. Behavioral parameters were analyzed using one-way or multiway ANOVAs followed by Tukey's or Fisher's least significant difference test for post hoc comparisons. Correlation analyses were conducted using Pearson correlation coefficients. The significance threshold was set at 0.05. Data collection and analyses were performed blinded to the conditions of the experiments.

Reporting Summary. Further information on research design is available in the Nature Research Reporting Summary linked to this article.

Data availability

The datasets generated and analyzed during the current study are available from the corresponding author upon reasonable request.

References

51. Capone, F., Bonsignore, L. T. & Cirulli, F. Methods in the analysis of maternal behavior in the rodent. *Curr. Protoc. Toxicol.* **Chapter 13**, Unit13.19 (2005).
52. Frau, R. et al. Sleep deprivation disrupts prepulse inhibition of the startle reflex: reversal by antipsychotic drugs. *Int. J. Neuropsychopharmacol.* **11**, 947–955 (2008).
53. Godar, S. C. et al. Maladaptive defensive behaviours in monoamine oxidase A-deficient mice. *Int. J. Neuropsychopharmacol.* **14**, 1195–1207 (2011).
54. Frau, R. et al. The neurosteroidogenic enzyme 5α-reductase mediates psychotic-like complications of sleep deprivation. *Neuropsychopharmacology* **42**, 2196–2205 (2017).
55. Bortolato, M., Godar, S. C., Davarian, S., Chen, K. & Shih, J. C. Behavioral disinhibition and reduced anxiety-like behaviors in monoamine oxidase B-deficient mice. *Neuropsychopharmacology* **34**, 2746–2757 (2009).

56. Paxinos, G. & Watson, C. *The Rat Brain in Stereotaxic Coordinates* (Academic, 2007).
57. Devoto, P., Flore, G., Longu, G., Pira, L. & Gessa, G. L. Origin of extracellular dopamine from dopamine and noradrenaline neurons in the medial prefrontal and occipital cortex. *Synapse* **50**, 200–205 (2003).
58. Melis, M., Camarini, R., Ungless, M. A. & Bonci, A. Long-lasting potentiation of GABAergic synapses in dopamine neurons after a single in vivo ethanol exposure. *J. Neurosci.* **22**, 2074–2082 (2002).
59. Johnson, S.W. & North, R. A. Two types of neurone in the rat ventral tegmental area and their synaptic inputs. *J. Physiol.* **450**, 455–468 (1992).
60. Ungless, M. A., Whistler, J. L., Malenka, R. C. & Bonci, A. Single cocaine exposure in vivo induces long-term potentiation in dopamine neurons. *Nature* **411**, 583–587 (2001).
61. Barna, L. et al. Correlated confocal and super-resolution imaging by VividSTORM. *Nat. Protoc.* **11**, 163–183 (2016).
62. Dani, A., Huang, B., Bergan, J., Dulac, C. & Zhuang, X. Superresolution imaging of chemical synapses in the brain. *Neuron* **68**, 843–856 (2010).
63. Huang, B., Jones, S. A., Brandenburg, B. & Zhuang, X. Whole-cell 3D STORM reveals interactions between cellular structures with nanometer-scale resolution. *Nat. Methods* **5**, 1047–1052 (2008).
64. Dudok, B. et al. Cell-specific STORM super-resolution imaging reveals nanoscale organization of cannabinoid signaling. *Nat. Neurosci.* **18**, 75–86 (2015).
65. Melis, M. et al. PPARα regulates cholinergic-driven activity of midbrain dopamine neurons via a novel mechanism involving α7 nicotinic acetylcholine receptors. *J. Neurosci.* **33**, 6203–6211 (2013).

nature research

Corresponding author(s): Miriam Melis

Last updated by author(s): Aug 1, 2019

Reporting Summary

Nature Research wishes to improve the reproducibility of the work that we publish. This form provides structure for consistency and transparency in reporting. For further information on Nature Research policies, see Authors & Referees and the Editorial Policy Checklist.

Statistics

For all statistical analyses, confirm that the following items are present in the figure legend, table legend, main text, or Methods section.

n/a	Confirmed	
☐	☒	The exact sample size (*n*) for each experimental group/condition, given as a discrete number and unit of measurement
☐	☒	A statement on whether measurements were taken from distinct samples or whether the same sample was measured repeatedly
☐	☒	The statistical test(s) used AND whether they are one- or two-sided *Only common tests should be described solely by name; describe more complex techniques in the Methods section.*
☒	☐	A description of all covariates tested
☐	☒	A description of any assumptions or corrections, such as tests of normality and adjustment for multiple comparisons
☐	☒	A full description of the statistical parameters including central tendency (e.g. means) or other basic estimates (e.g. regression coefficient) AND variation (e.g. standard deviation) or associated estimates of uncertainty (e.g. confidence intervals)
☐	☒	For null hypothesis testing, the test statistic (e.g. *F*, *t*, *r*) with confidence intervals, effect sizes, degrees of freedom and *P* value noted *Give P values as exact values whenever suitable.*
☒	☐	For Bayesian analysis, information on the choice of priors and Markov chain Monte Carlo settings
☒	☐	For hierarchical and complex designs, identification of the appropriate level for tests and full reporting of outcomes
☐	☒	Estimates of effect sizes (e.g. Cohen's *d*, Pearson's *r*), indicating how they were calculated

Our web collection on statistics for biologists contains articles on many of the points above.

Software and code

Policy information about availability of computer code

Data collection	pClamp v10.2, excel (microsoft windows v8.0), NIS-Elements AR with N-STORM module v4.3
Data analysis	Clampfit v10.6.0.13, Huygens v4.2.1, vividSTORM v1.5, ImageJ, Photoshop vCS5, GraphPad v6.0 (Prism), Statistica v13 (Statsoft), Mini Analysis Program v6.0.3 (Synaptosoft)

For manuscripts utilizing custom algorithms or software that are central to the research but not yet described in published literature, software must be made available to editors/reviewers. We strongly encourage code deposition in a community repository (e.g. GitHub). See the Nature Research guidelines for submitting code & software for further information.

Data

Policy information about availability of data

All manuscripts must include a data availability statement. This statement should provide the following information, where applicable:

- Accession codes, unique identifiers, or web links for publicly available datasets
- A list of figures that have associated raw data
- A description of any restrictions on data availability

The datasets generated and analysed during the current study are available from the corresponding author on reasonable request.

Field-specific reporting

Please select the one below that is the best fit for your research. If you are not sure, read the appropriate sections before making your selection.

☒ Life sciences ☐ Behavioural & social sciences ☐ Ecological, evolutionary & environmental sciences

Life sciences study design

All studies must disclose on these points even when the disclosure is negative.

Sample size	No statistical methods (e.g. G*Power or similar software) were used to determine sample size. The sample size estimates were based on our numerous previous studies on the field.
Data exclusions	Esclusion criteria were pre-established when statistical outliers were identified by the Grubb's test (setting the alpha at 0.05).
Replication	All attempts at replication were successful when experiments were carried out from different litters and at different times (i.e., months, years).
Randomization	Animals were randomly assigned to each group at prenatal treatment group (always with a different code) and at any experimental procedure.
Blinding	Investigators were blind to group allocation during the execution of experiments, and data analyses. Code was broken after the analyses were completed.

Reporting for specific materials, systems and methods

We require information from authors about some types of materials, experimental systems and methods used in many studies. Here, indicate whether each material, system or method listed is relevant to your study. If you are not sure if a list item applies to your research, read the appropriate section before selecting a response.

Materials & experimental systems

n/a	Involved in the study
☐	☒ Antibodies
☒	☐ Eukaryotic cell lines
☒	☐ Palaeontology
☐	☒ Animals and other organisms
☒	☐ Human research participants
☒	☐ Clinical data

Methods

n/a	Involved in the study
☒	☐ ChIP-seq
☒	☐ Flow cytometry
☒	☐ MRI-based neuroimaging

Antibodies

Antibodies used	Primary Antibodies: Bassoon: Millipore, ABN255, lot.Q2564148, 1:1000; Tyrosine Hydroxylase (TH): Immunostar, 22941, lot.1552001, 1:5000; Abcam ab76442; Vesicular Inhibitory Amino Acid Transporter (VIAAT): Synaptic Systems, 131 004, 1:2000; 131 003, 1:500; Vesicular Glutamate Transporter 1 (vGluT1): Synaptic Systems, 135 304, 1:5000; Cannabinoid receptor type 1: ImmunoGenes, 1:1000. Secondary antibodies: Alexa647-conjugated anti-rabbit, donkey Jackson, 711-605-152 1:400; Alexa647-conjugated anti-guinea-pig, donkey, Jackson, 706-605-148, 1:400; Alexa594-conjugated anti-rabbit, donkey, Jackson, 711-595-152, 1:400; Alexa488-conjugated anti-mouse, donkey Jackson, 715-545-150, 1:400; DyLight405-conjugated anti-mouse, donkey, Jackson, 715-475-151, 1:400; CF568-conjugated anti-guinea pig, donkey Biotium, 20377-50ul, 1:1000.
Validation	Bassoon: rabbit, evaluated by Western Blotting in mouse brain tissue lysate and by IHC in rat brain samples by the supplier. Tyrosine Hydroxylase (TH): Quality control tested with IHC on rat catecholamine neuron systems by the supplier. Vesicular Inhibitory Amino Acid Transporter (VIAAT): Guinea pig, KO verified by the supplier, specific in rat, mouse, and zebrafish. Vesicular Inhibitory Amino Acid Transporter (VIAAT): Rabbit, KO verified by the supplier, specific in human, rat mouse and monkey. Vesicular Glutamate Transporter 1 (vGluT1): Guinea pig, KO verified by the supplier, specific in rat, mouse, human and cow. Cannabinoid receptor type 1: Rabbit, Dudok et al. 2015. Nature Neuroscience, KO verified by reference. Anti-tyrosine hydroxylase: Chicken, verified in IHC, ICC, IF by the supplier.

Animals and other organisms

Policy information about studies involving animals; ARRIVE guidelines recommended for reporting animal research

Laboratory animals	We used male and female Sprague-Dawley outbred rats (Hsd:Sprague Dawley® SD®, Envigo, Italy) age PND 14-28; Long Evans tyrosine hydroxylase (TH)-Cre recombinase rats (bred on-site, at the University of Baltimore, Maryland, USA).
Wild animals	The study did not involve wild animals.
Field-collected samples	The study did not involve samples collected from the field.

Ethics oversight	All procedures were performed in accordance with the European legislation EU Directive 2010/63 and the National Institute of Health Guide for the Care and Use of Laboratory Animals and were approved by the Animal Ethics Committees of the University of Cagliari and by Italian Ministry of Health (auth. n. 659/2015-PR and 725/2019-PR) and by the Institutional Animal Use and Care Committee at the University of Maryland (0617002).

Note that full information on the approval of the study protocol must also be provided in the manuscript.